Oligomer formation from the gas-phase reactions of Criegee intermediates with hydroperoxide esters: mechanism and kinetics

Long Chen,[1,2] Yu Huang,*[,1,2] Yonggang Xue,[1,2] Zhihui Jia,[3] Wenliang Wang[4]

[1] *State Key Lab of Loess and Quaternary Geology (SKLLQG), Institute of Earth Environment, Chinese Academy of Sciences (CAS), Xi'an, 710061, China*

[2] *CAS Center for Excellence in Quaternary Science and Global Change, Xi'an, 710061, China*

[3] *School of Materials Science and Engineering, Shaanxi Normal University, Xi'an, Shaanxi, 710119, China*

[4] *School of Chemistry and Chemical Engineering, Key Laboratory for Macromolecular Science of Shaanxi Province, Shaanxi Normal University, Xi'an, Shaanxi, 710119, China*

Submitted to *Atmospheric Chemistry & Physics*

*Corresponding author:

Prof. Yu Huang, E-mail address: huangyu@ieecas.cn

Abstract

Hydroperoxide esters, formed in the reactions of carbonyl oxides (also called Criegee intermediates, CIs) with formic acid, play a crucial role in the formation of secondary organic aerosol (SOA) in the atmosphere. However, the transformation mechanism of hydroperoxide esters in the presence of stabilized Criegee intermediates (SCIs) is not well understood. Herein, the oligomerization reaction mechanisms and kinetics of distinct SCIs (CH_2OO, syn-CH_3CHOO, $anti$-CH_3CHOO and $(CH_3)_2COO$) reactions with their respective hydroperoxide esters as well as with hydroperoxymethyl formate (HPMF) are investigated in the gas phase using quantum chemical and kinetics modeling methods. The calculations show that the addition reactions of SCIs with hydroperoxide esters proceed through successive insertion of SCIs into hydroperoxide ester to form oligomers that involve SCIs as the repeated chain unit. The exothermicity of oligomerization reactions significantly decreases when the number of methyl substituents increases, and the exothermicity of $anti$-methyl substituted carbonyl oxides is obviously higher than that of syn-methyl substituted carbonyl oxides. The –OOH insertion reaction is energetically more feasible than the –CH insertion pathway in the SCIs oligomerization reactions, and the barrier heights increase with increasing the number of SCIs added to the oligomer except syn-CH_3CHOO. For the reactions of distinct SCIs with HPMF, the barrier of -OOH insertion pathway shows a dramatic decrease when a methyl substituent occurs at the $anti$-position, while it reveals a significant increase when a methyl group is introduced at the syn-position and dimethyl substituent. Compared with the rate coefficients of the CH_2OO + HPMF reaction, the rate coefficients increase by about one order of magnitude when a methyl substituent occurs at the $anti$-position, whereas the rate coefficients decrease by 1-2 orders of magnitude when a methyl group is introduced at the syn-position. These new findings advance our current understanding on the influence of Criegee-chemistry on the formation processes and chemical compositions of SOA.

1. Introduction

Alkenes are an important class of volatile organic compounds (VOCs) that are emitted into the atmosphere from large quantities of biogenic and anthropogenic sources (Lester and Klippenstein, 2018). The reaction with ozone is one of the dominant degradation pathways for alkenes in the atmosphere (Johnson and Marston, 2008; Atkinson and Arey, 2003). Ozonolysis of alkene proceeds through the electrophilic 1,3-cycloaddition of ozone to C=C bond of alkenes to form a primary ozonides (POZ), and then it rapidly decomposes into a carbonyl compound and a carbonyl oxide (also called Criegee intermediates, CIs) (Criegee, 1975; Osborn and Taatjes, 2015; Giorio et al., 2017). A part of the initially energized CIs (~ 37-50%) may promptly dissociate to OH radicals, which are thought to be an important nonphotolytic source of OH radicals in the atmosphere (Novelli et al., 2014; Liu et al., 2014). The remaining CIs (~ 63-50%) are collisionally stabilized prior to the thermal unimolecular decay (Lester and Klippenstein, 2018; Novelli et al., 2014; Anglada and Solé, 2016). The stabilized Criegee intermediates (SCIs) can proceed bimolecular reactions with various trace species such as H_2O, NO_2, SO_2, and HCOOH to generate secondary organic aerosol (SOA), thus profoundly influencing air quality, global climate and human health (Osborn and Taatjes, 2015; Khan et al., 2018; Lin and Chao, 2017; Liu et al., 2019; Chhantyal-Pun et al., 2018; Gong and Chen, 2021; Taatjes, 2017).

Formic acid (HCOOH), one of the most abundant carboxylic acids, has a significant influence on rainwater acidity in remote areas, where pH reduces by 0.25-0.5 in the presence of HCOOH (Stavrakou et al., 2012; Wang et al., 2020; Chaliyakunnel et al., 2016). It also plays an important role in the formation of cloud condensation nuclei (CCN), indirectly influencing radiative forcing and climate change (Yu, 2000). The primary sources of HCOOH include biomass burning, human activities, tropical and boreal forests, as well as the secondary sources involve the photochemical oxidation of non-methane hydrocarbons, such as ketene-enols, vinyl alcohol, isoprene, and terpenoids (Stavrakou et al., 2012; Wang et al., 2020; Chaliyakunnel et al., 2016; So et al., 2014; Paulot et al., 2011). According to satellite measurements, the production

of HCOOH is up to 100-120 Tg yr^{-1}, and the value is expected to increase due to the acceleration of industrialization and urbanization (Stavrakou et al., 2012). Recent kinetics measurements have revealed that the reaction with HCOOH is a more important loss process for SCI than is presently assumed, especially in terrestrial equatorial areas and in high SCI concentration areas (Welz et al., 2014; Chung et al., 2019). The formed hydroperoxide esters have been identified as the low-volatility and high-oxygenated compounds, contributing to the formation and growth of SOA (Welz et al., 2014; Vansco et al., 2021; Sakamoto et al., 2017; Riva et al., 2017).

Welz et al. (2014) directly determined the rate coefficients for the reactions of CH_2OO and CH_3CHOO with formic and acetic acid by employing multiplexed photoionization mass spectrometry and cavity-enhanced broadband ultraviolet absorption spectroscopy. They found that the measured rate coefficients are in the excess of 1.0×10^{-10} cm^3 molecule^{-1} s^{-1}, which are several orders of magnitude greater than those derived from previous experimental studies (Johnson et al., 2001; Tobias and Ziemann, 2001). Sipilä et al. (2014) conducted a competitive reaction kinetics experiment to investigate the reactions of acetone oxide (($CH_3)_2OO$) with SO_2, HCOOH and CH_3COOH, and they concluded that the rate coefficients of the ($CH_3)_2OO$ + HCOOH/CH_3OOH reactions are faster than that of the ($CH_3)_2OO$ + SO_2 system by about three times. These high rate coefficients could make the reaction with carboxylic acids a substantial dominant chemical sink for carbonyl oxides in the atmosphere (Welz et al., 2014; Taatjes et al., 2019; Chhantyal-Pun et al., 2017). Quantum chemical calculations show that the reaction of CH_2OO with HCOOH proceeds through a facile transfer of hydrogen atom from the acidic OH group to the terminal oxygen of CH_2OO to form hydroperoxymethyl formate (HPMF) (Long et al., 2009; Vereecken, 2017; Porterfield et al., 2019). Chen et al. (2018) concluded the same by investigating the reactions of various carbonyl oxides with HCOOH that the barrierless 1,4-insertion reaction is the most favorable pathway, and the primary products are hydroperoxide esters. Caravan et al. (2020) employed high-level ab initio CCSD(T)-F12 methods to study the reaction of methyl vinyl ketone oxide (MVK-oxide) with HCOOH, and they

found that the barrierless net insertion of MVK-oxide into HCOOH leading to the formation of a functionalized hydroperoxide is dominant over fragmentation to produce an alkoxy radical and OH radicals. Moreover, oligomerization reactions with hydroperoxides and peroxy radicals are identified as one of the dominant loss processes for carbonyl oxides under atmospheric conditions (Sakamoto et al., 2013; Sadezky et al., 2008; Zhao et al., 2015; Chen et al., 2017 and 2019). All the above milestone investigations provide important information for understanding the chemistry of Criegee intermediate in the presence of carboxylic acids. However, to the best of our knowledge, there are few studies on the oligomerization reactions of SCIs with hydroperoxide esters, which are important with regard to organic new particle and cloud condensation nuclei formations. Moreover, the relationship between the reactivity of SCIs and the nature of substituents remains uncertain in the SCIs oligomerization reactions.

In the present study, we mainly focus on the oligomerization reaction mechanisms and kinetics of four carbonyl oxides reactions with their respective hydroperoxide esters as well as with HPMF by employing quantum chemical calculations and kinetics modeling methods. For the initiation reactions of carbonyl oxides with formic acid, four kinds of pathways including 1,4 O-H insertion, 1,2 O-H insertion, C-H insertion, and C=O cycloaddition are considered. For the oligomerization reactions of the successive insertion of carbonyl oxides into hydroperoxide esters, two types of reactions involving –OOH and –CH insertions are taken into account. The selected carbonyl oxides, including CH_2OO, *syn*-, *anti*-CH_3CHOO and $(CH_3)_2CHOO$, are anticipated upon the ozonolysis of ethylene, propylene, and 2,3-dimethyl-2-butene, whereas the hydroperoxide esters are assumed to arise from the bimolecular reactions of carbonyl oxides with formic acid in the atmosphere.

2. Computational details

2.1 Electronic structure and energy calculations

The geometries of all stationary points, including reactants (R), intermediates (IM), transition states (TS), and products (P), are optimized at the M06-2X/6-311+G(2df,2p)

level of theory, since the M06-2X functional has the reliable performance for predicting thermochemistry, kinetics and hydrogen bonding interactions (Zhao and Truhlar, 2008). Harmonic vibrational frequencies are performed at the same level to verify the nature of transition state (NIMAG = 1) and minimum (NIMAG = 0), and to provide zero-point vibrational energy (ZPVE) and Gibbs free energies corrections (G_{corr}), which are scaled by a factor of 0.98 (Alecu et al., 2010). Intrinsic reaction coordinate (IRC) calculations are carried out to verify that each transition state is connected to the desired reactant and product (Fukui, 1981). The single point energy (SPE) calculations are performed at the M06-2X/ma-TZVP level of theory based on the M06-2X/6-311+G(2df,2p) optimized geometries. Moreover, the basis set superposition error (BSSE) is performed by using the counterpoise method proposed by Boys and Bernardi (1970) to evaluate the stability of the pre-reactive complex (RC). Herein, the Gibbs free energy (G) is defined as the sum of SPE and Gibbs correction ($G = E + G_{corr}$). Electronic energy ($\Delta E^{\neq}$) and Gibbs free energy ($\Delta G^{\neq}$) barriers are defined as the difference in energy between a TS and a RC ($\Delta E^{\neq} = E_{TS} - E_{RC}$ and $\Delta G^{\neq} = G_{TS} - G_{RC}$). Reaction Gibbs free energy (ΔG) is defined as the difference in energy between a P and a R ($\Delta G = G_P - G_R$).

To further assess the reliability of the selected M06-2X/ma-TZVP method for SPE calculations, the single point energies of all stationary points involved in the initiation reactions of distinct SCIs with HCOOH are recalculated at the high-accuracy CCSD(T)/6-311+G(2df,2p) and QCISD(T)/6-311+G(2df,2p) levels of theory. The calculated results are summarized in Table S1. This table shows that the $\Delta E^{\neq}$ and $\Delta G^{\neq}$ obtained using the QCISD(T) method are in excellent agreement with those obtained using the CCSD(T) approach. It is therefore that the energies obtained using the CCSD(T) method are used as the benchmark for comparison. The mean absolute deviations (MAD) of $\Delta E^{\neq}$ and $\Delta G^{\neq}$ between the CCSD(T) and M06-2X methods are 0.43 and 0.41 kcal mol^{-1}, respectively; the largest deviations of $\Delta E^{\neq}$ and $\Delta G^{\neq}$ are 1.0 and 1.1 kcal mol^{-1}, respectively. These results reveal that the energies obtained using the M06-2X method are close to those obtained using the CCSD(T) approach. Therefore, the M06-2X/ma-TZVP method is suitable to investigate the SCIs

oligomerization reactions. In the following discussion, the energies are applied in terms of Gibbs free energy to describe the reaction mechanism unless otherwise stated. All electronic structure calculations are carried out by using Gaussian 09 program (Frisch et al., 2009). The Multiwfn program and Visual molecular dynamics (VMD) are utilized to analysis and visualize the molecular orbitals of the relevant species (Lu and Chen, 2012).

2.2 Kinetics calculations

The rate coefficients for the barrierless reactions are determined by employing the inverse Laplace transformation (ILT) method. The ILT calculations are performed with the MESMER 6.0 program (Glowacki et al., 2012). In the ILT treatment, the rotational constants, vibrational frequencies, molecular weights, energies and other input parameters are obtained from the M06-2X/6-311+G(2df,2p) or M06-2X/ma-TZVP methods. For the barrierless reaction of 1,4 O-H insertion of SCIs into HCOOH, SCIs and HCOOH are assigned as the deficient and excess reactants, respectively. The concentration of HCOOH is given a value of 5.0×10^{10} molecules cm^{-3} in the simulation, which is taken from the typical concentration of HCOOH in the tropical forest environments (Vereecken et al., 2012). N_2 is applied as the buffer gas. A single exponential down model is employed to simulate the collision transfer ($<\Delta E>_{down} = 200$ cm^{-1}). The collisional Lennard-Jones parameters are estimated with the empirical formula described by Gilbert and Smith (1990).

The rate coefficients for the bimolecular reactions with the tight transition states are calculated by using the canonical transition state theory (CTST) along with one-dimensional asymmetric Eckart tunneling correction (Truhlar et al., 1996; Eckart, 1930). The CTST/Eckart calculations are performed with the KiSThelP 2019 program (Canneaux et al., 2013). As shown in Fig. 1, the entrance pathway Entry2 of R_1R_2COO reaction with HCOOH consists of two steps: (i) an intermediate IMent2 is formed via a barrierless process; (ii) then, it rearranges to the product Pent2 through a tight transition state TSent2. The whole reaction process can be described as Eq. (1):

$$R_1R_2COO + HCOOH \underset{k_{-1}}{\overset{k_1}{\rightleftharpoons}} IMent2 \xrightarrow{k_2} Pent2 \tag{1}$$

Assuming the rapid equilibrium is established between the IMent2 and reactants. According to the steady-state approximation (SSA), the total rate coefficient is approximately expressed as Eq. (2) (Zhang et al., 2012):

$$k_{tot} = \frac{k_1}{k_{-1} + k_2} k_2 \approx \frac{k_1}{k_{-1}} k_2 = K_{eq}k_2 \tag{2}$$

The equilibrium constant K_{eq} is written as Eq. (3):

$$K_{eq} = \sigma \frac{Q_{IM}(T)}{Q_{R1}(T)Q_{R2}(T)} \exp\left(\frac{G_R - G_{IM}}{RT}\right) \tag{3}$$

where σ refers to reaction symmetry number, $Q_{IM}(T)$, $Q_{R1}(T)$ and $Q_{R2}(T)$ denote the partition functions of intermediate, reactants R1 and R2, which are equal to the multiplication of translational, rotational, vibrational and electronic partition functions ($Q = Q_{rot}Q_{vib}Q_{trans}Q_{elec}$) (Mendes et al., 2014), T is the temperature in Kelvin, R is the ideal gas constant, G_R and G_{IM} are the total Gibbs free energies of reactant and intermediate, respectively.

3. Results and discussion

3.1 Initiation reactions of distinct SCIs with HCOOH

The reaction with HCOOH is one of the dominant loss processes for SCIs and is expected to trigger the formation of SOA in the atmosphere (Chhantyal-Pun et al., 2018; Cabezas and Endo, 2020; Zhao et al., 2018; Zhou et al., 2019). The potential energy surface (PES) of distinct SCIs (CH$_2$OO, *syn*-, *anti*-CH$_3$CHOO and (CH$_3$)$_2$COO) reactions with HCOOH is drawn in Fig. 1. The geometries of all stationary points are displayed in Fig. S1. The relative free energy of each stationary point and free energy barrier ($\Delta G^{\neq}$) of each elementary reaction are summarized in Table 1. As shown in Fig. 1, the bimolecular reaction of distinct SCIs with HCOOH proceeds via four possible pathways, namely (1) 1,4 O-H insertion (Entry 1), (2) 1,2 O-H insertion (Entry 2), (3) C-H insertion (Entry 3), and (4) C=O cycloaddition (Entry 4). For Entry 1, the addition reaction of CH$_2$OO with HCOOH proceeds through the 1,4 O-H insertion of CH$_2$OO

into HCOOH to form a hydroperoxide ester HC(O)O-CH$_2$OO-H with a exoergicity of 37.6 kcal·mol^{-1}. The formation of HC(O)O-CH$_2$OO-H is obtained through a concerted process of O$_2$-H$_2$ bond breaking in the HCOOH and O$_4$-H$_2$ and C$_2$-O$_1$ bonds forming. Despite an attempt by various methods, the corresponding transition state is still not located in the effort of optimization. To further validate the barrierless process of 1,4 O-H insertion reaction, a relaxed scan over the O$_4$-H$_2$ and C$_2$-O$_1$ bonds is performed at the M06-2X/6-311+G(2df,2p) level of theory. The scans start from the optimized structure of the adduct product HC(O)O-CH$_2$OO-H, and the O$_4$-H$_2$ and C$_2$-O$_1$ bond length are then increased in steps of 0.10 Å. The relaxed scan energy profiles are presented in Fig. S2. As seen in Fig. S2a, the relative energy of the minimum energy path from reactant to product decreases monotonically when the bond length of O$_4$-H$_2$ and C$_2$-O$_1$ bonds decreases, suggesting that the transition state is not exist in the 1,4 O-H insertion reaction of CH$_2$OO with HCOOH. Similar conclusion is also obtained from the relaxed scan energy profiles for the HCOOH + *anti*-CH$_3$CHOO, HCOOH + *syn*-CH$_3$CHOO and HCOOH + (CH$_3$)$_2$COO (Fig. S2b-d) reactions that 1,4 O-H insertion reactions are barrierless. This conclusion is further supported by the analogous reaction systems that 1,4 O-H insertion reactions of carbonyl oxides with carboxylic acids are a barrierless process including concerted hydrogen atom transfer and new C-O bond formation (Chhantyal-Pun et al., 2017; Long et al., 2009; Vereecken, 2017; Cabezas and Endo, 2019; Lin et al., 2019).

The exothermicity of 1,4 O-H insertion reactions of distinct SCIs with HCOOH is assessed by the reaction enthalpy ($\Delta_r H_{298}^o$), which is defined as the difference between the enthalpies of formation ($\Delta_f H_{298}^o$) of the products and reactants ($\Delta_r H_{298}^o = \sum_{products} \Delta_f H_{298}^o - \sum_{reactants} \Delta_f H_{298}^o$). To the best of our knowledge, there are no literature values available on the enthalpies of formation of carbonyl oxides and hydroperoxide esters except the simplest carbonyl oxide CH$_2$OO. Therefore, the isodesmic reaction method is adopted to obtain the enthalpies of formation, and the results are listed in Table S2. An isodesmic reaction is a hypothetical reaction, in which the type of

248   chemical bonds in the reactants is the similar as that of chemical bonds in the products.

249   The following isodesmic reaction is constructed because the experimental values of H_2,

250   CH_4 and H_2O are available ($\Delta_f H_{298}^o$ (H_2) = 0.00 kcal·mol^{-1}; $\Delta_f H_{298}^o$ (CH_4) = -17.82

251   kcal·mol^{-1}; $\Delta_f H_{298}^o$ (H_2O) = -57.79 kcal·mol^{-1}).

$$SCIs + nH_2 \rightarrow CH_4 + mH_2O \tag{4}$$
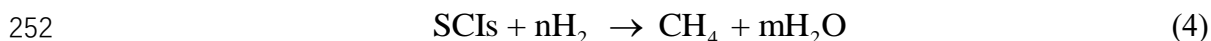
253   As seen in Table S2, the enthalpy of formation of CH_2OO is calculated to be 23.23

254   kcal·mol^{-1}, which is in good agreement with the available literature values (Chen et al.,

255   2016; Karton et al., 2013). This result implies that the theoretical method employed

256   herein is reasonable to predict the thermochemical parameters. The enthalpies of

257   formation of carbonyl oxides and hydroperoxide esters significantly decrease with

258   increasing the number of methyl groups. Notably, the decreased values in the enthalpies

259   of formation of carbonyl oxides are greater than those of hydroperoxide esters under

260   the condition of the same number of methyl groups. For example, the enthalpy of

261   formation of *anti*-CH_3CHOO decreases by 12.95 kcal·mol^{-1} compared to the enthalpy

262   of formation of CH_2OO, and the enthalpy of formation of Pent1b decreases by 12.12

263   kcal·mol^{-1} compared to the enthalpy of formation of Pent1a. The reaction enthalpies

264   decrease in the order of -44.69 (CH_2OO + HCOOH → Pent1a) < -43.86 (*anti*-

265   CH_3CHOO + HCOOH → Pent1b) < -38.13 (*syn*-CH_3CHOO + HCOOH → Pent1c) < -

266   37.12 kcal·mol^{-1} ((CH_3)$_2$COO + HCOOH → Pent1d), indicating that the reaction

267   enthalpies are highly dependent on the number and location of methyl groups. The trend

268   in reaction enthalpies is consistent with the trend in the enthalpies of formation of

269   carbonyl oxides. The reason might be attributed to the decreased values in the enthalpies

270   of formation of carbonyl oxides greater than those of hydroperoxide esters under the

271   condition of the same number of methyl groups.

272   For Entry 2, each addition reaction starts with the formation of a pre-reactive

273   hydrogen bonded complex IMent2 in the entrance channel. Then it immediately

274   converts into product Pent2 through the 1,2 O-H insertion transition state. The

275   formation of Pent2 is obtained via a concerted process of O_2-H_2 bond rupture in the

HCOOH and O_4-H_2 and C_2-O_2 bonds forming. The reaction barrier $\Delta G^{\neq}$ increases in the order of 10.0 (CH_2OO) < 13.0 (*anti*-CH_3CHOO) < 14.6 (*syn*-CH_3CHOO) ≈ 14.4 ((CH_3)$_2$COO) kcal·mol^{-1}, suggesting that the parent CH_2OO + HCOOH reaction is favored kinetically. Compared with the barrier of the parent system, the barrier increases by 3.0 kcal·mol^{-1} when a methyl substitution occurs at the R_1 position, and the barrier increases by ~ 5 kcal·mol^{-1} when a methyl group is introduced at the R_2 position and dimethyl substituent. The aforementioned result implies that the methyl-substituted CH_2OO hinders the 1,2 O-H insertion of carbonyl oxides into formic acid. Notably, the exothermicity decreases significantly as the number of methyl group is increased. The products Pent1 and Pent2 formed from Entry 1 and 2 are two conformations that differ in the orientation of the –C(O)H moiety over the –OOH group. The calculated result shows that Pent1 is more stable than Pent2 in energy due to the existence of intramolecular hydrogen bond between hydrogen atom of –OOH group and carbonyl oxygen atom.

For Entry 3, the addition reaction begins with the formation of a pre-reactive complex IMent3 in the entrance channel, and then it surmounts a barrier to reaction. However, the barriers of C-H insertion reactions are significantly high (21.8-27.6 kcal·mol^{-1}), such that they are of less importance in the atmosphere. The high reaction barriers might be attributed to the large bond dissociation energy (BDE) of C-H bond in the formic acid. For Entry 4, the addition reaction proceeds through a cyclization process of C_2-O_1 and O_4-C_1 bond forming to produce a five-membered ring compound Pent4. The barrier of C=O cycloaddition reaction in the CH_2OO + HCOOH reaction is 5.8 kcal·mol^{-1}, which is lower than that of the corresponding channels in Entry 2 and Entry 3 by 4.2 and 16.0 kcal·mol^{-1}, respectively. The result reveals that the C=O cycloaddition reaction is feasible kinetically. A similar conclusion is also obtained from the reactions of HCOOH with *syn*-, *anti*-CH_3CHOO and (CH_3)$_2$COO that the C=O cycloaddition reactions are favored over 1,2 O-H and C-H insertion reactions.

The rate coefficients of each elementary pathway included in the initiation reactions of distinct SCIs with HCOOH are calculated in the temperature range of 273-

400 K, as listed in Table S3-S6. As shown in Table S3, the total rate coefficients $k_{tot\text{-}CH2OO}$ of CH_2OO reaction with HCOOH are in excess of 1.0×10^{-10} cm^3 molecule^{-1} s^{-1}, and they exhibit a slightly negative temperature dependence in the temperature range studied. $k_{tot\text{-}CH2OO}$ is estimated to be 1.4×10^{-10} cm^3 molecule^{-1} s^{-1} at 298 K, which is in good agreement with the experimental values reported by Welz et al. (2014) ([1.1 ± 0.1] $\times 10^{-10}$), Chung et al. (2019) ([1.4 ± 0.3] $\times 10^{-10}$), and Peltola et al. (2020) ([1.0 ± 0.03] $\times 10^{-10}$). $k(TS_{ent1})$ is approximately equal to $k_{tot\text{-}CH2OO}$ in the whole temperature range, and it decreases in the range of 1.7×10^{-10} (273 K) to 1.2×10^{-10} (400 K) cm^3 molecule^{-1} s^{-1} with increasing temperature. $k(TS_{ent1})$ is several orders of magnitude greater than $k(TS_{ent2})$, $k(TS_{ent3})$ and $k(TS_{ent4})$ over the temperature range from 273 to 400 K. The result again shows that the barrierless 1,4 O-H insertion reaction is predominant. The calculated $K_{eq\text{-}ent2}$, $k_{2\text{-}ent2}$, and $k(TS_{ent2})$ ($k(TS_{ent2}) = K_{eq\text{-}ent2} \times k_{2\text{-}ent2}$) in Entry 2 are listed in Table S7. This table shows that $K_{eq\text{-}ent2}$ significantly decreases with increasing temperature, and $k_{2\text{-}ent2}$ increases as the temperature is increased. However, the decreased value in $K_{eq\text{-}ent2}$ is greater than the increased value in $k_{2\text{-}ent2}$ under the same temperature range. For example, $K_{eq\text{-}ent2}$ deceases by a factor of 6.3 and $k_{2\text{-}ent2}$ increases by a factor of 2.9 at 298 K compared with the values of $K_{eq\text{-}ent2}$ and $k_{2\text{-}ent2}$ at 273 K. It is therefore that $k(TS_{ent2})$ decreases with the temperature increasing. Similar conclusion is also obtained from the results of the rate coefficients in Entry 4 that $k(TS_{ent4})$ exhibits a negative temperature dependence in the temperature range studied (Table S8). The aforementioned results imply that $k(TS_{ent2})$ and $k(TS_{ent4})$ are mediated by the pre-reactive complexes IMent2 and IMent4 in the Entry 2 and 4. It should be noted that although the barrier of Entry 2 is 4.2 kcal·mol^{-1} higher than that of Entry 4, $k(TS_{ent2})$ is merely about 1-2 fold smaller than $k(TS_{ent4})$. The reason is ascribed to the fact that the C=O cycloaddition reaction is entropically unfavorable (Vereecken, 2017).

Equivalent to the case of CH_2OO reaction with HCOOH, the rate coefficient of each elementary pathway involved in the *anti*-CH_3CHOO + HCOOH reaction also decreases with the temperature increasing (Table S4). This table shows that Entry 1 is kinetically favored over Entry 2, 3 and 4, and Entry 2 is competitive with Entry 4 in the

range 273-400 K. Similar conclusion is also obtained from the results of the rate coefficients for the reactions of *syn*-CH$_3$CHOO and (CH$_3$)$_2$COO with HCOOH that Entry 1 is the dominant pathway (Table S5-S6). It deserves mentioning that the competition of Entry 2 is significantly greater than that of Entry 4 in the *syn*-CH$_3$CHOO + HCOOH and (CH$_3$)$_2$COO + HCOOH systems. Based on the above discussions, it can be concluded that the relative importance of different pathways is highly dependent on the number and location of methyl substituents in the carbonyl oxides. Notably, the rate coefficient of each elementary pathway included in the *anti*-CH$_3$CHOO + HCOOH reaction is several orders of magnitude greater than that of the corresponding channel involved in the other SCIs + HCOOH systems. It is because that *anti*-CH$_3$CHOO is substantially more reactive toward HCOOH than other SCIs. Similar phenomenon has also observed from the reactivity of *anti*-CH$_3$CHOO toward water and SO$_2$ (Taatjes et al., 2013; Long et al., 2016; Huang et al., 2015; Cabezas and Endo, 2018). At ambient temperature, the total rate coefficients of HCOOH reactions with *anti*-CH$_3$CHOO, *syn*-CH$_3$CHOO and (CH$_3$)$_2$COO are estimated to be 5.9, 2.7 and 4.8 × 10^{-10} cm^3 molecule^{-1} s^{-1}, respectively, which are consistent with the prior experimental measurements of 5 ± 3, 2.5 ± 0.3 and 4.5 × 10^{-10} cm^3 molecule^{-1} s^{-1} (Welz et al., 2014; Chung et al., 2019; Sipilä et al., 2014).

In summary, the barrierless 1,4 O-H insertion reaction is the dominant pathway in the initiation reactions of distinct SCIs with HCOOH. This conclusion is consistent with the recent experimental results derived from the reactions of formic acid with methacrolein oxide (MACR-OO) and methyl vinyl ketone oxide (MVK-OO) that the 1,4-addition mechanism is energetically favorable (Vansco et al., 2021; Caravan et al., 2020). Therefore, in the present study, the adduct products Pent1 formed form the barrierless 1,4 O-H insertion of carbonyl oxides into HCOOH are selected as the model compounds to investigate the oligomerization reaction mechanisms of carbonyl oxides reactions with hydroperoxide esters.
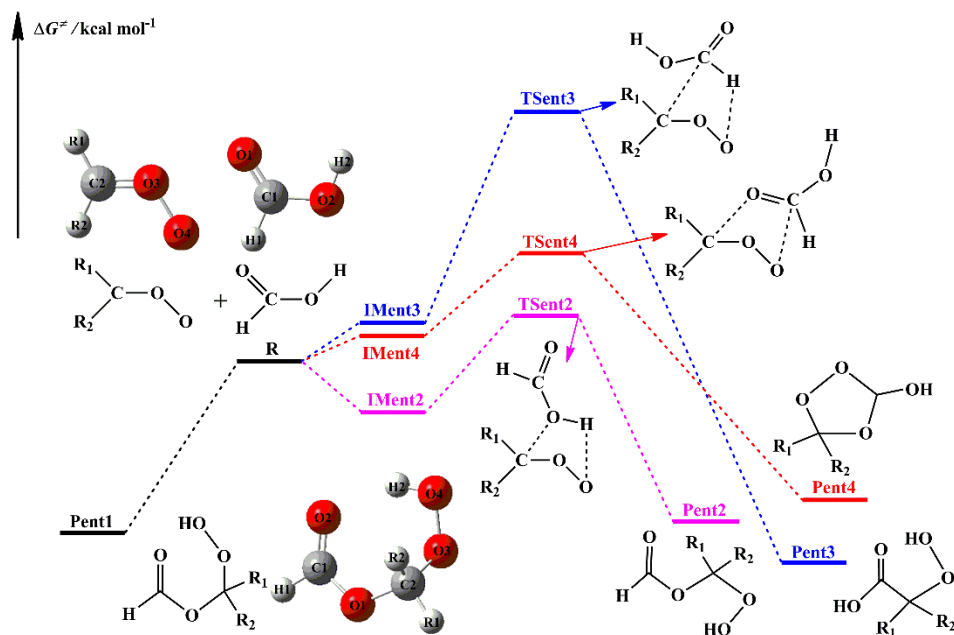
361

362 **Figure 1.** Schematic PES for the possible entrance pathways of the initiation reactions of HCOOH

363 with various SCIs (black, pink, blue, and red lines represent 1,4 O-H insertion, 1,2 O-H insertion,

364 C-H insertion, and C=O cycloaddition reactions, respectively)

365 **Table 1** Relative free energies of stationary points and free-energy barriers ($\Delta G^{\neq}$) at 298 K in kcal

366 mol^{-1} for the various SCIs (R_1R_2COO, R_1, R_2=H, CH_3) reactions with HCOOH calculated at the

367 M06-2X/ma-TZVP//M06-2X/6-311+G(2df,2p) level of theory

Entry	R1	R2	IMent	TSent	Pent	$\Delta G^{\neq}$
1	H	H	–	–	-37.6	–
	CH₃	H	–	–	-34.0	–
	H	CH₃	–	–	-29.8	–
	CH₃	CH₃	–	–	-25.6	–
2	H	H	-3.1	6.9	-37.3	10.0
	CH₃	H	-11.0	2.0	-33.7	13.0
	H	CH₃	-6.6	8.0	-29.1	14.6
	CH₃	CH₃	-8.8	5.6	-24.9	14.4
3	H	H	3.4	25.2	-46.9	21.8
	CH₃	H	1.8	24.0	-41.5	22.2
	H	CH₃	3.0	30.6	-37.6	27.6
	CH₃	CH₃	1.9	29.5	-33.0	27.6
4	H	H	3.4	9.2	-31.7	5.8
	CH₃	H	2.2	7.8	-29.4	5.6
	H	CH₃	3.5	14.6	-25.3	11.1
	CH₃	CH₃	3.0	13.2	-22.9	10.2

368 ## 3.2. The reactions of distinct SCIs with their respective hydroperoxide

369 ## esters

The formed hydroperoxide ester has two possible unimolecular decay pathways. The first is the direct O-O bond rupture resulting in the formation of oxylmethylformate and OH radicals (Vereecken, 2017). The second is the –OH fragment binding to adjacent hydrogen atom leading to the formation of anhydride and H_2O (Aplincourt and Ruiz-López, 2000; Neeb et al., 1998). However, the barriers of these two unimolecular reactions are extremely high, such that they are of less importance in the atmosphere. The formed hydroperoxide ester possess –OOH and –OC(O)H groups, both of them can serve as the reactive moieties to react with carbonyl oxides giving rise to the formation of oligomers. In the present study, we mainly consider two types of pathways: (a) –OOH insertion and (b) –CH insertion, while the C=O cycloaddition reaction is not taken into account because it is entropically unfavorable (Vereecken, 2017; Lin, et al., 2019). The aforementioned reactions are discussed in detail in the following subsections.

3.2.1 The reactions of 2CH₂OO with Pent1a

The simplest carbonyl oxide, CH_2OO, originates from the reaction of all terminal alkenes with ozone (ozonolysis) in the atmosphere (Lin and Chao, 2017). The reaction with HCOOH is expected to be one of the dominant loss processes for CH_2OO, and the main product is Pent1a (also called as HPMF) (Welz et al., 2014; Cabezas and Endo, 2019). A schematic PES for the addition reaction $2CH_2OO$ + Pent1a is drawn in Fig. 2, and the optimized geometries of all stationary points are displayed in Fig. S3. As seen in Fig. 2, the successive insertion of CH_2OO into Pent1a eventually leads to the formation of oligomers P2a and P2b composed of CH_2OO as the repeat unit. These oligomerization reactions are strongly exothermic and spontaneous (> 83 kcal·mol^{-1}), implying that they are feasible thermodynamically.

The addition reaction $2CH_2OO$ + Pent1a initially proceeds through two possible pathways, namely (1) –OOH insertion reaction R1a, and (2) –CH insertion reaction R1b. For the –OOH insertion reaction R1a, the pre-reactive intermediate IM1a with a seven-membered ring structure is formed in the entrance channel, which is stabilized by the hydrogen bond interactions between the H_4 atom of Pent1a and the O_6 atom of CH_2OO

$(D_{(O6-H4)} = 1.706$ Å$)$, and between the H_6 atom of CH_2OO and the O_3 atom of Pent1a $(D_{(O3-H6)} = 2.115$ Å$)$. Then IM1a converts into P1a $(C_3H_6O_6$, $HC(O)O–(CH_2OO)_2–H)$ via a concerted process of O_4-H_4 bond breaking in the Pent1a and O_4-C_3 and H_4-O_6 bonds forming with a barrier of 8.1 kcal·mol^{-1}. For the –CH insertion reaction R1b, the pre-reactive intermediate IM1b with a seven-membered ring structure is formed in the entrance channel, which is stabilized by the van der Waals (vdW) interactions between the O_3 atom of Pent1a and the C_3 atom of CH_2OO $(D_{(O3-C3)} = 2.602$ Å$)$, and between the O_6 atom of CH_2OO and the C_1 atom of Pent1a $(D_{(O6-C1)} = 2.608$ Å$)$. Due to the absence of hydrogen bond in IM1b, the energy of IM1b is lower than that of IM1a by 3.0 kcal·mol^{-1}. IM1b transforms into P1b $(C_3H_6O_6$, $HO_2CH_2OC(O)CH_2OOH)$ via a concerted process of C_1-H_1 bond breaking in the Pent1a and C_1-C_3 and H_1-O_6 bonds forming with a barrier of 21.5 kcal·mol^{-1}. By comparing the barriers of R1a and R1b, it can be concluded that the –OOH insertion reaction is favored over the –CH insertion reaction. The high reaction barrier of R1b is attributed to the large bond dissociation energy (BDE) of C-H bond in the Pent1a. To further insight into the reaction mechanism of R1a, the natural bond orbital (NBO) analysis of the donor-acceptor orbitals involved in the TS1a is performed using the M06-2X wave function. The possible donor-acceptor interactions are estimated by using the second order perturbation theory. As illustrated in Fig. S4, the strong interactions are identified as the interaction of the lone pair orbital of O_6 atom and the antibonding orbital of O_4-H_4 bond, and the interaction of the lone pair orbital of O_4 atom and the antibonding orbital of C_3-O_5 bond.

Similarly, the addition reaction CH_2OO + P1a proceeds through the formation of the pre-reactive intermediates IM2a and IM2b in the entrance channel, which are stabilized by a hydrogen bond between the terminal oxygen atom of CH_2OO and the reacting hydrogen atom of P1a, and a van der Waals (vdW) interaction between the central carbon atom of CH_2OO and the carbonyl oxygen atom of P1a. The relative energies of IM2a and IM2b with respect to the separate reactants P1a and CH_2OO are -1.2 and 3.2 kcal·mol^{-1}, respectively, below the energies of the initial reactants $2CH_2OO$ and Pent1a are 41.6 and 37.2 kcal·mol^{-1}, respectively. Then they immediately transform

428 into the respective products P2a and P2b through the –OOH and –CH insertion
429 transition states TS2a and TS2b with the barriers of 10.1 and 21.6 kcal·mol⁻¹. This result
430 again shows that the –OOH insertion reaction is favored kinetically. It deserves
431 mentioning that the barrier of –OOH insertion reaction increases as the number of
432 CH₂OO is increased. From the viewpoint of the geometrical parameters of TS2a and
433 TS2b, the breaking O-H and C-H bonds are elongated by 14.8% and 20.6%,
434 respectively, with respect to the equilibrium structures of IM2a and IM2b, while the
435 forming C-O and C-C bond length are 2.013 and 2.264 Å, respectively. The result
436 reveals that TS2a and TS2b are structurally reactant-like, which are consistent with the
437 Hammond's hypothesis that the earlier transition states are generally exothermic
438 (Hammond, 1955).
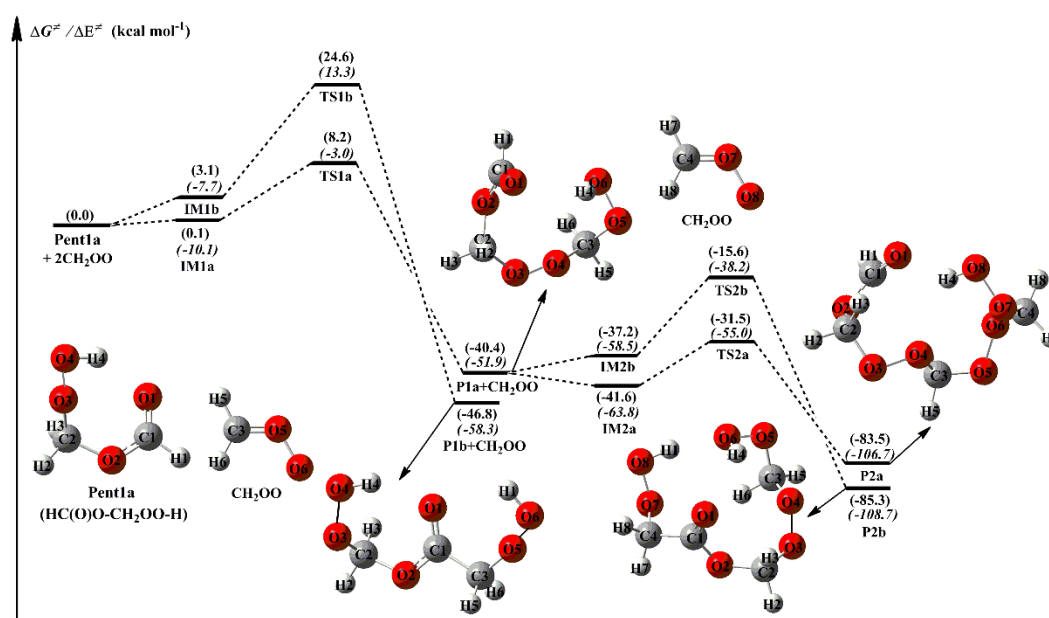
439

440 **Figure 2.** PES (Δ*G* and Δ*E*, in italics) for the 2CH₂OO + Pent1a reaction at the M06-2X/ma-
441 TZVP//M06-2X/6-311+G(2df,2p) level of theory

3.2.2 The reactions of *anti*-CH₃CHOO with Pent1b

443   The methyl-substituted CH₂OO has two conformers, *syn*- and *anti*-CH₃CHOO that
444 distinguish by the orientation of methyl group relative to the terminal oxygen (Taatjes
445 et al., 2013). *syn*-CH₃CHOO is more stable than *anti*-CH₃CHOO in energy due to the
446 existence of intramolecular hydrogen bond (Long et al., 2016). The activation enthalpy
447 of the interconversion between *syn*-CH₃CHOO and *anti*-CH₃CHOO is up to 38.5
448 kcal·mol⁻¹, implying that they can treat as independent species in the atmosphere (Long

449 et al., 2016; Yin and Takahashi, 2017). A schematic PES for the addition reaction 2*anti*-

450 CH_3CHOO + Pent1b is presented in Fig. 3, and the optimized geometries of all

451 stationary points are shown in Fig. S5. As shown in Fig. 3, the addition reaction 2*anti*-

452 CH_3CHOO + Pent1b proceeds through successive insertion of *anti*-CH_3CHOO into

453 Pent1b leading to the formation of oligomers P4a and P4b that contain *anti*-CH_3CHOO

454 as chain unit. The first *anti*-CH_3CHOO addition reaction begins with the formation of

455 IM3a and IM3b in the entrance channel, which lie -2.2 and 2.4 kcal·mol^{-1} respectively,

456 with respect to the separate reactants. Then the IM3a and IM3b transform into P3a and

457 P3b via –OOH and –CH insertion transition states TS3a and TS3b with the barriers of

458 5.6 and 20.3 kcal·mol^{-1}. This result shows that the –OOH insertion reaction is more

459 favorable than the –CH insertion pathway. Compared with the barriers of R1a and R1b

460 in the 2CH_2OO + Pent1a reaction, the barriers of R3a and R3b decrease by 2.5 and 1.2

461 kcal·mol^{-1} when a methyl group is introduced at the *anti*-position. The result reveals

462 that the reactivity of *anti*-CH_3CHOO is substantially higher than that of CH_2OO. This

463 conclusion is further supported by the findings of other studies, which have reported

464 that *anti*-CH_3CHOO is more reactive toward H_2O, SO_2, and H_2O_2 than CH_2OO (Chen

465 et al., 2017; Taatjes et al., 2013; Huang et al., 2015). Similarly, the secondary *anti*-

466 CH_3CHOO addition reaction starts with the formation of IM4a and IM4b in the entrance

467 channel with the 0.1 and 3.7 kcal·mol^{-1} stability, followed by conversion to the final

468 products P4a and P4b through the –OOH and –CH insertion reactions R4a and R4b.

469 The transition states TS4a and TS4b lie 7.0 and 21.0 kcal·mol^{-1}, respectively, above the

470 energies of the respective intermediates IM4a and IM4b. This result again shows that

471 the –OOH insertion reaction is the most favorable channel, and the barrier increases as

472 the number of *anti*-CH_3CHOO is increased.
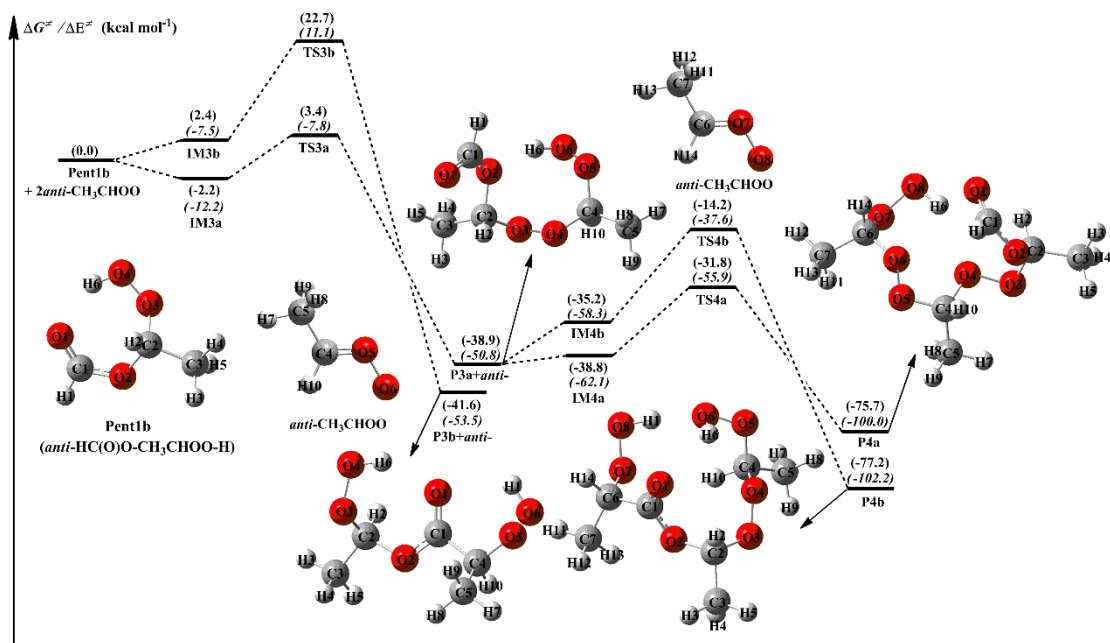
473

474 **Figure 3.** PES (ΔG and ΔE, in italics) for the 2*anti*-CH₃CHOO + Pent1b reaction at the M06-

475 2X/ma-TZVP//M06-2X/6-311+G(2df,2p) level of theory

3.2.3 The reactions of *syn*-CH₃CHOO with Pent1c

477 Equivalent to the 2*anti*-CH₃CHOO + Pent1b reaction, the addition reaction 2*syn*-

478 CH₃CHOO + Pent1c has similar transformation pathways, and is thus briefly discussed

479 in the present study. From Fig. 4, it can be seen that the addition reaction 2*syn*-

480 CH₃CHOO + Pent1c undergoes via successive insertion of *syn*-CH₃CHOO into Pent1c

481 to form P6a and P6b that involve *syn*-CH₃CHOO as the repeating unit. The most

482 favorable pathway is that the breakage of O₄-H₆ bond in the –OOH group of Pent1c

483 occurs simultaneously with the insertion of first *syn*-CH₃CHOO into Pent1c to form

484 P5a, followed by the insertion of secondary *syn*-CH₃CHOO into P5a to produce P6a.

485 The barriers of these two –OOH insertion reactions R5a and R6a are 13.8 and 11.8

486 kcal·mol⁻¹, respectively, which are higher than those of R3a and R4a in the 2*anti*-

487 CH₃CHOO + Pent1b system by 8.2 and 4.8 kcal·mol⁻¹, respectively. The result reveals

488 that the reactivity of *syn*-CH₃CHOO is substantially lower than that of *anti*-CH₃CHOO.

489 Notably, the barrier of the favorable –OOH insertion pathway decreases with increasing

490 the number of *syn*-CH₃CHOO in the 2*syn*-CH₃CHOO + Pent1c reaction, which is

491 contrary to the case of the 2CH₂OO + Pent1a and 2*anti*-CH₃CHOO + Pent1b reactions.
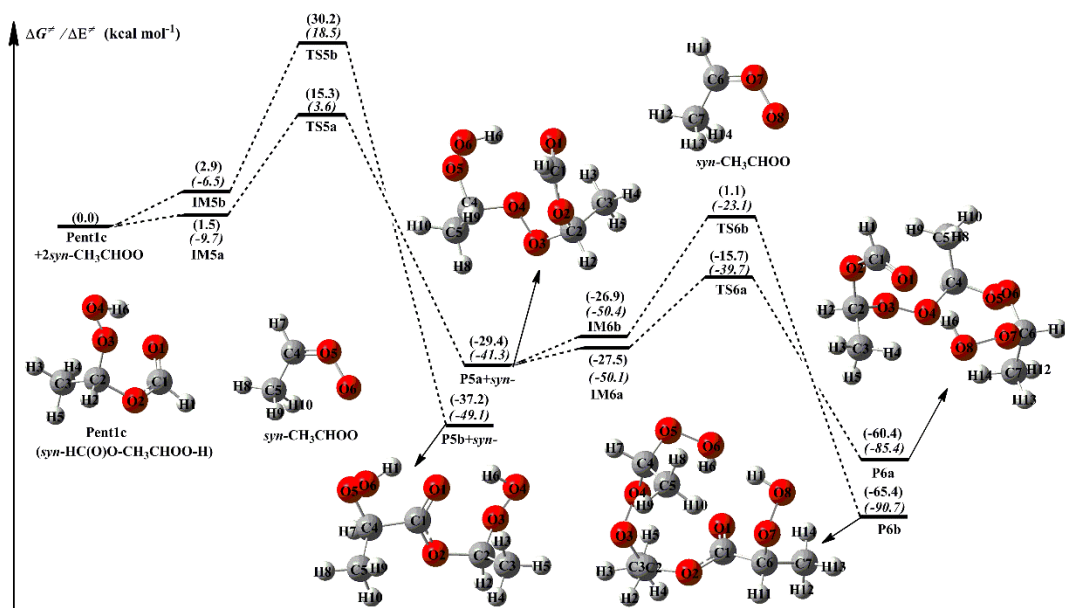
492

493 **Figure 4.** PES (ΔG and ΔE, in italics) for the 2*syn*-CH$_3$CHOO + Pent1c reaction at the M06-

494 2X/ma-TZVP//M06-2X/6-311+G(2df,2p) level of theory

3.2.4 The reactions of 2(CH$_3$)$_2$COO with Pent1d

496   The dimethyl-substituted Criegee intermediate, (CH$_3$)$_2$COO, is generated from the

497 ozonolysis of 2,3-dimethyl-2-butene in the atmosphere (Lester and Klippenstein, 2018;

498 Drozd et al., 2017; Long et al., 2018). The bimolecular reaction of (CH$_3$)$_2$COO with

499 water is not fast enough ($k < 1.5 \times 10^{-16}$ cm^3 molecule^{-1} s^{-1}), while the reaction of

500 (CH$_3$)$_2$COO with HCOOH has a near gas kinetic limit rate ($k = 5.4 \times 10^{-10}$ cm^3 molecule$^-$

501 ^{1} s^{-1}) (Huang et al., 2015). The result implies that a fraction of (CH$_3$)$_2$COO may survive

502 under high humidity environments and react with HCOOH leading to the formation of

503 hydroperoxide ester Pent1d. A schematic PES for the addition reaction 2(CH$_3$)$_2$COO +

504 Pent1d is plotted in Fig. 5, and the optimized geometries of all stationary points are

505 shown in Fig. S7.

506   As seen in Fig. 5, the addition reaction 2(CH$_3$)$_2$COO + Pent1d starts with the

507 formation of complexes IM7a and IM7b, which lie 1.9 and 2.4 kcal·mol^{-1}, respectively,

508 above the energies of the separate reactants. Then they subsequently transform into

509 products P7a and P7b through the –OOH and –CH insertion transition states TS7a and

510 TS7b with the barriers of 12.2 and 26.4 kcal·mol^{-1}. This result again shows that the –

511 OOH insertion reaction is favored over the –CH insertion pathway. A similar conclusion

512 is also obtained from the secondary (CH$_3$)$_2$COO addition reaction that the –OOH

insertion reaction is the dominant pathway. It is of interest to compare the barriers of –OOH insertion reactions in the $(CH_3)_2COO$ + Pent1d system with those of the analogous reactions in other SCIs + Pent1 reactions. It can be found that the barriers decrease in the order of syn-CH_3CHOO > $(CH_3)_2COO$ > CH_2OO > $anti$-CH_3CHOO in the first-step SCIs addition reaction, while they become $(CH_3)_2COO$ > syn-CH_3CHOO > CH_2OO > $anti$-CH_3CHOO in the second-step SCI addition pathway. The result shows that the reactivity of SCIs is significantly affected by the number and location of methyl substituents. A similar conclusion is also obtained from the thermodynamic parameters that the exothermicity of –OOH insertion reactions significantly decreases with increasing the number of methyl substituents, and the exothermicity of $anti$-methyl substituted carbonyl oxide is obviously higher than that of syn-methyl substituted carbonyl oxide.
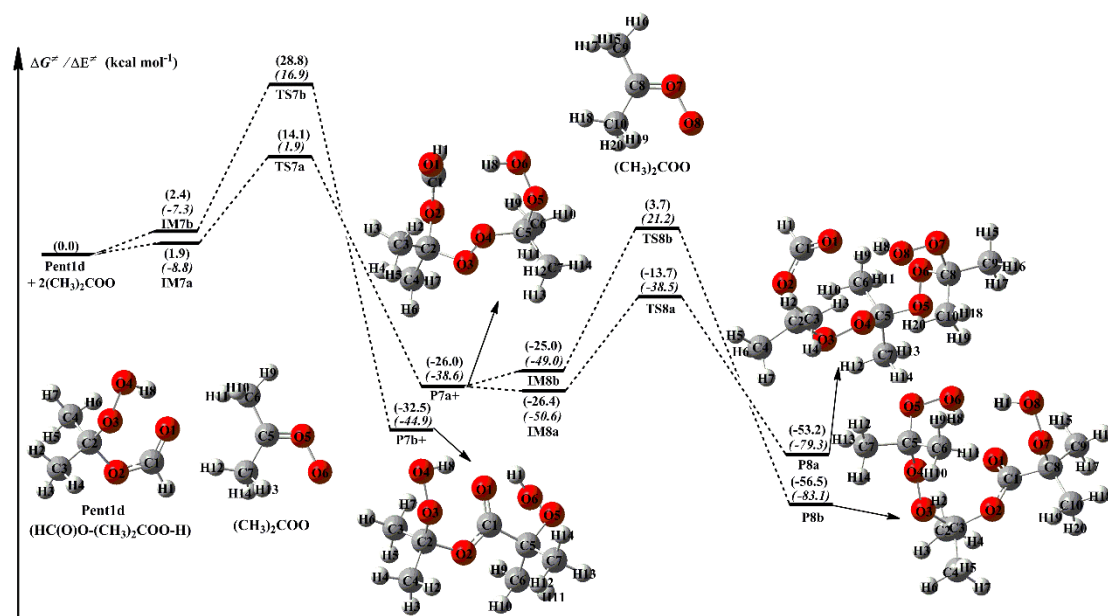
Figure 5. PES (ΔG and ΔE, in italics) for the $2(CH_3)_2COO$ + Pent1d reaction at the M06-2X/ma-TZVP//M06-2X/6-311+G(2df,2p) level of theory.

3.3 The reactions of distinct SCIs with Pent1a and implications in atmospheric chemistry

To further elucidate the effect of the number and location of methyl substituents on the reactivity of carbonyl oxides toward hydroperoxide esters, Pent1a (also called as HPMF) is selected as the model compound since it is the simplest hydroperoxide ester

533 formed from the barrierless reaction of 1,4 O-H insertion of CH_2OO into HCOOH. As

534 mentioned above, –OOH insertion reaction in the oligomerization reactions is the most

535 favorable pathway. Therefore, this type of reaction is merely considered in the reactions

536 of distinct SCIs with Pent1a. The corresponding PES and the optimized geometries of

537 all stationary points are displayed in Figs. 6 and S8, respectively. As seen in Fig. 6, each

538 pathway starts with the formation of a pre-reactive intermediate, and then it overcomes

539 a modest barrier to reaction. The barrier of the reaction of CH_2OO with Pent1a is

540 calculated to be 8.1 $kcal \cdot mol^{-1}$, which is higher than that of the *anti*-CH_3CHOO +

541 Pent1a reaction by 2.5 $kcal \cdot mol^{-1}$. The reason of low barrier can be explained by the

542 NPA atomic charges, as presented in Fig. S9. As seen in Fig. S9, the charges of the

543 central carbon atom C_1 and the terminal oxygen atom O_1 of CH_2OO are 0.186e and -

544 0.459e, respectively, indicating that CH_2OO is indeed a zwitterion. The C_1 atom charge

545 becomes more positive (0.393e), while the O_1 atom charge becomes more negative (-

546 0.497e) when a methyl substituent occurs at the *anti*-position. This result suggests that

547 the *anti*-methyl substituent enhances the characteristic of carbonyl oxides zwitterion

548 and reduces the reaction barriers. Compared with the barrier of the CH_2OO + Pent1a

549 reaction, the barriers increase by about 3.0 $kcal \cdot mol^{-1}$ when a methyl group is

550 introduced at the *syn*-position and dimethyl substituent. Although *syn*-methyl and

551 dimethyl substituent promote the raise of carbonyl oxides zwitterion, the steric

552 hindrance effect and intramolecular hydrogen bond are obviously dominant for *syn*-

553 CH_3CHOO and $(CH_3)_2COO$, that are not thus conducive to the nucleophilic attack of

554 hydroperoxide esters. It is worth noting that the exothermicity of distinct SCIs reactions

555 with Pent1a obviously decreases as the number of methyl group is increased, and the

556 exothermicity of *anti*-methyl substituent is higher than that of *syn*-methyl substituent.

557 The rate coefficients of distinct SCIs reactions with Pent1a are calculated in the

558 temperature range of 273-400 K as summarized in Table S9. This table shows that the

559 rate coefficients k_{R1a} of the CH_2OO + Pent1a reaction (R1a) decrease in the range of

560 5.0×10^{-11} (273 K) to 5.0×10^{-12} cm^3 $molecule^{-1}$ s^{-1} (400 K) with increasing temperature.

561 A similar phenomenon is also observed from the rate coefficients of Pent1a reactions

with *anti*-CH$_3$CHOO (R9), *syn*-CH$_3$CHOO (R10), and (CH$_3$)$_2$COO (R11) that they exhibit a slightly negative temperature dependence. k_{R9} is several orders of magnitude greater than k_{R1a}, k_{R10} and k_{R11} in the whole temperature range, suggesting that the bimolecular reaction *anti*-CH$_3$CHOO + Pent1a (R9) is favored kinetically. Compared with the rate coefficients of R1a, the rate coefficients increase by about one order of magnitude when a methyl substituent occurs at the *anti*-position, whereas the rate coefficients decrease by 1 to 2 orders of magnitude when a methyl group is introduced at the *syn*-position. It should be noted that although the barrier of R10 is nearly identical to that of R11, k_{R10} is 1 to 2 orders of magnitude lower than k_{R11} in the entire temperature range. This is probably because the rate coefficients are mediated by pre-reactive intermediates that IM11 is more stable than IM10 in energy.

It is of interest to assess whether the reactions of distinct SCIs with HPMF can compete well with the losses to reactions with trace species (e.g., H$_2$O, HCOOH and SO$_2$), because it is well known that the reactions with trace species are expected to be the dominant chemical sinks for SCIs in the atmosphere (Taatjes et al., 2013; Long et al., 2016). The reported concentrations of coreactant, the rate coefficients k, and the effective pseudo-first-order rate constants ($k_{\mathrm{eff}} = k$[coreactant]) for distinct SCI reactions with H$_2$O, HCOOH, SO$_2$, and HPMF are summarized in Table 2. As seen in Table 2, the rate coefficient of a particular SCI reaction with trace species is strongly dependent on its structure. The methyl group substitution may alter the rate coefficient by several to tens of times. The atmospheric concentrations of H$_2$O, HCOOH and SO$_2$ in the tropical forest environments are measured to be 3.9-6.1 × 10^{17}, 5.0-10 × 10^{10}, and 1.7-9.0 × 10^{10} molecules cm^{-3}, respectively (Vereecken, 2012). For the reactions of CH$_2$OO with H$_2$O, HCOOH, and SO$_2$, the experimental rate coefficients are determined to be < 1.5 × 10^{-15}, [1.1 ± 0.1] × 10^{-10}, and [3.9 ± 0.7] × 10^{-11} cm^3 molecule^{-1} s^{-1}, respectively (Welz et al., 2012 and 2014; Chao et al., 2015), which translate into $k_{\mathrm{eff(CH2OO+H2O)}}$, $k_{\mathrm{eff(CH2OO+HCOOH)}}$ and $k_{\mathrm{eff(CH2OO+SO2)}}$ of 5.9-9.2 × 10^2, 5.5-11, and 0.7-3.5 s^{-1}, respectively. The result reveals that the reaction of CH$_2$OO with H$_2$O is the most important bimolecular reaction. $k_{\mathrm{eff(CH2OO+HCOOH)}}$ is greater by a factor of 3-8 than

$k_{\text{eff(CH2OO+SO2)}}$, indicating that the reaction of CH_2OO with HCOOH is favored over reaction with SO_2. Similar conclusion is also obtained from the results of k_{eff} for the reactions of *anti*-CH_3CHOO, *syn*-CH_3CHOO and $(CH_3)_2COO$ with H_2O, HCOOH and SO_2 that SCIs reactions with H_2O are faster than with HCOOH, which, in turn, are faster than with SO_2.

According to the results shown in the Table 2, the room temperature rate coefficient for the reaction of CH_2OO with HPMF is calculated to be 2.7×10^{-11} cm^3 molecule^{-1} s^{-1}. However, to the best of our knowledge, the atmospheric concentration of HPMF has not been reported up to now. If we assume that the concentration of HPMF is the same as that of HCOOH, $k_{\text{eff(CH2OO+HPMF)}}$ is estimated to be 1.4-2.7 s^{-1}, which is significantly lower than $k_{\text{eff(CH2OO+H2O)}}$ and $k_{\text{eff(CH2OO+HCOOH)}}$. $k_{\text{eff(CH2OO+HPMF)}}$ is nearly identical to $k_{\text{eff(CH2OO+SO2)}}$, indicating that the CH_2OO + HPMF reaction is competitive with the CH_2OO + SO_2 system. Previous model-measurement studies have estimated the surface-level SCIs concentrations in the range of 1.0×10^4 to 1.0×10^5 molecules cm^{-3} (Khan et al., 2018; Novelli et al., 2017). If we assume that the concentration of HPMF is equal to that of SCIs, $k_{\text{eff(CH2OO+HPMF)}}$ is calculated to be $2.7\text{-}27 \times 10^{-7}$ s^{-1}, which is several orders of magnitude lower than $k_{\text{eff(CH2OO+H2O)}}$, $k_{\text{eff(CH2OO+HCOOH)}}$ and $k_{\text{eff(CH2OO+SO2)}}$. This result indicates that the reaction of CH_2OO with HPMF is of less importance. Similar conclusion is also obtained from the reactions of *anti*-CH_3CHOO, *syn*-CH_3CHOO and $(CH_3)_2COO$ with HPMF.

To further evaluate the relative importance of the complex SCIs reactions with coreactant, the bimolecular reactions of methyl vinyl ketone oxide (MVK-OO) with H_2O, HCOOH, SO_2, and HPMF are considered. MVK-OO, formed with 21 to 23% yield from the ozonolysis of isoprene, is a four carbon, asymmetric, resonance-stabilized Criegee intermediate (Barber et al., 2018). MVK-OO has four conformers, *syn-trans*-, *syn-cis*-, *anti-trans*-, and *anti-cis*- as shown in Fig. S10. Herein, *syn* and *anti* refer to the orientation of the –CH_3 group relative to the terminal oxygen of MVK-OO, whereas *cis* and *trans* refer to the orientation of the $C_8=C_9$ bond relative to the $C_1=O_2$ bond. According to the results shown in the Fig. S10, the lowest-energy conformer is

syn-trans-MVK-OO, which is lower than *syn-cis-*, *anti-trans-*, and *anti-cis*-MVK-OO by 1.42, 2.43 and 2.69 kcal·mol⁻¹, respectively. Therefore, the lowest-energy conformer *syn-trans*-MVK-OO is selected as the model compound to study its bimolecular reactions. As shown in Table 2, the rate coefficient of H_2O reaction with *syn-trans*-MVK-OO is lower than with other SCIs by 2 to 3 orders of magnitude. The reason is likely to be that the existence of methyl and vinyl groups hinders the occurrence of bimolecular reaction with water vapour. Consequently, a fraction of *syn-trans*-MVK-OO may survive in the presence of water vapour and react with other species. $k_{eff(MVK-OO+H2O)}$ is nearly identical to $k_{eff(MVK-OO+HCOOH)}$, which is greater than $k_{eff(MVK-OO+SO2)}$ and $k_{eff(MVK-OO+HPMF)}$ when the concentration of HPMF is the same as that of HCOOH. $k_{eff(MVK-OO+H2O)}$ and $k_{eff(MVK-OO+HCOOH)}$ are greater than $k_{eff(MVK-OO+SO2)}$, which, in turn, are greater than $k_{eff(MVK-OO+HPMF)}$ when the concentration of HPMF is equal to that of SCIs. Based on the above discussions, it can be concluded that the relative importance of carbonyl oxides reactions with hydroperoxide esters is significantly dependent on the concentrations of hydroperoxide esters. These reactions may play a certain role in the formation of organic new particle in some regions where low concentration of water vapour and high concentration of hydroperoxide esters occur.
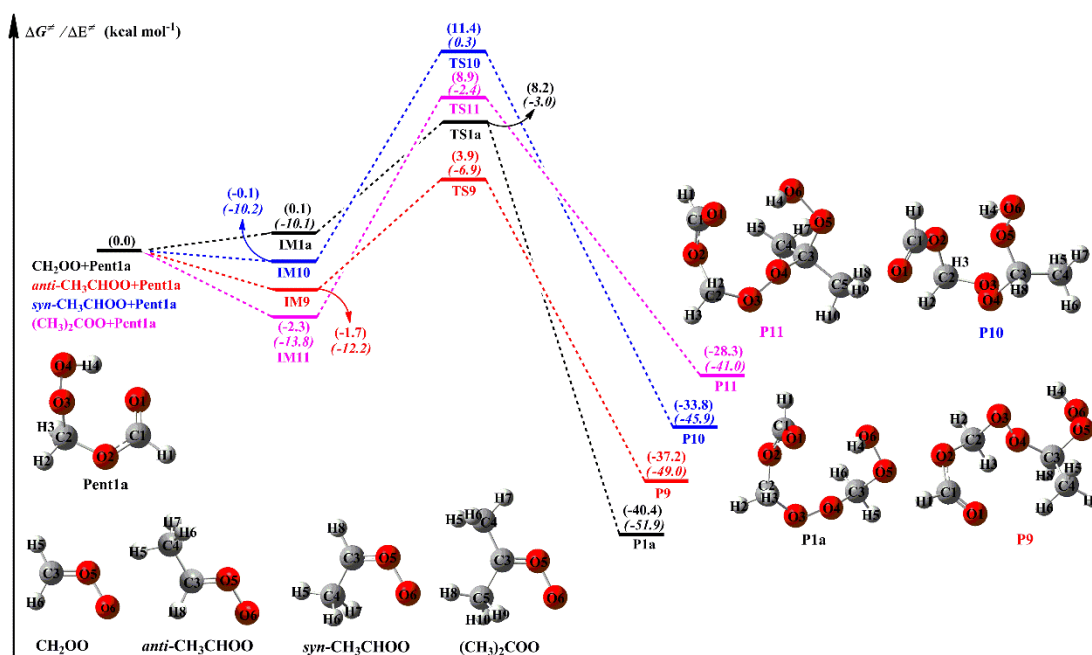
Figure 6. PES (ΔG and ΔE, in italics) for the distinct SCIs + Pent1a reactions at the M06-2X/ma-TZVP//M06-2X/6-311+G(2df,2p) level of theory

Table 2 The reported concentrations of coreactant, the rate coefficients k, and the effective pseudo-first-order rate constants ($k_{eff} = k$[coreactant]) for distinct SCI reactions with HPMF, H_2O, HCOOH and SO_2 at the tropical forest environments

SCIs	Coreactant	[Coreactant] (molecules cm^{-3})	k (cm^3 molecule^{-1} s^{-1})	k_{eff} (s^{-1})	Reference
CH$_2$OO	H$_2$O	3.9-6.1 × 10^{17}	< 1.5 × 10^{-15}	5.9-9.2 × 10^2	Chao et al., (2015)
	HCOOH	5.0-10.0 × 10^{10}	[1.1 ± 0.1] × 10^{-10}	5.5-11	Welz et al., (2014)]
	SO$_2$	1.7-9.0 × 10^{10}	[3.9 ± 0.7] × 10^{-11}	0.7-3.5	Welz et al., (2012)
	HPMF	-	2.7 × 10^{-11}	-	This work
anti-CH$_3$CHOO	H$_2$O	3.9-6.1 × 10^{17}	[1.0 ± 0.4] × 10^{-14}	3.9-6.1 × 10^3	Taatjes et al., (2013)
	HCOOH	5.0-10.0 × 10^{10}	[5 ± 3] × 10^{-10}	25.0-50.0	Welz et al., (2014)
	SO$_2$	1.7-9.0 × 10^{10}	[6.7 ± 1.0] × 10^{-11}	1.1-6.0	Taatjes et al., (2013)
	HPMF	-	3.3 × 10^{-10}	-	This work
syn-CH$_3$CHOO	H$_2$O	3.9-6.1 × 10^{17}	< 4.0 × 10^{-15}	1.6-2.4 × 10^3	Taatjes et al., (2013)
	HCOOH	5.0-10.0 × 10^{10}	[2.5 ± 0.3] × 10^{-10}	12.5-25.0	Welz et al., (2014)
	SO$_2$	1.7-9.0 × 10^{10}	[2.4 ± 0.3] × 10^{-11}	0.4-2.2	Taatjes et al., (2013)
	HPMF	-	1.7 × 10^{-13}	-	This work
(CH$_3$)$_2$COO	H$_2$O	3.9-6.1 × 10^{17}	< 1.5 × 10^{-16}	58.5-91.5	Huang et al., (2015)
	HCOOH	5.0-10.0 × 10^{10}	4.5 × 10^{-10}	22.5-45.0	Sipilä et al., (2014)
	SO$_2$	1.7-9.0 × 10^{10}	1.3 × 10^{-10}	2.2-11.7	Huang et al., (2015)
	HPMF	-	2.2 × 10^{-11}	-	This work
syn-trans-MVK-OO	H$_2$O	3.9-6.1 × 10^{17}	< 4.0 × 10^{-17}	15.6-24.4	Caravan et al., (2020)
	HCOOH	5.0-10.0 × 10^{10}	[3.0 ± 0.1] × 10^{-10}	15.0-30.0	Caravan et al., (2020)
	SO$_2$	1.7-9.0 × 10^{10}	[4.2 ± 0.6] × 10^{-11}	0.7-3.8	Caravan et al., (2020)

HPMF	-	3.0×10^{-11}	-	This work

3.4 Vapour pressure and volatility of adduct products

The assessment of Barley and McFiggans (2010) and O'Meara et al. (2014) found that the combination of boiling point estimation from Nannoolal et al. (2004) and vapour pressure estimation from Nannoolal et al. (2008) gives the lowest mean bias error of vapour pressure for atmospherically relevant compounds. Therefore, the saturated vapour pressure (P^0) of adduct products at room temperature is estimated by using the Nannoolal-Nannoolal method, and the results are listed in Table S10. From Table S10, it can be seen that the P^0 of adduct products involved in the successive reactions of CH_2OO with HCOOH increases first and then decreases with increasing the number of CH_2OO. The P^0 of the adduct product $HC(O)O(CH_2OO)_3H$ is maximum when the number of CH_2OO is equal to three. The P^0 of adduct products included in the successive reactions of $anti$-CH_3CHOO with HCOOH decreases significantly as the number of $anti$-CH_3CHOO is increased. Similar phenomenon is also observed from the successive reactions of syn-CH_3CHOO and $(CH_3)_2COO$ with HCOOH. Notably, the P^0 of adduct products decreases obviously when the size of SCIs increases. For example, the P^0 of the adduct product $HC(O)O(CH_2OO)_3H$ in the nCH_2OO + HCOOH reaction is estimated to be 4.43×10^{-3} atm, which is greater than those of the corresponding adduct products in the $nanti$-CH_3CHOO + HCOOH (7.12×10^{-4}), $nsyn$-CH_3CHOO + HCOOH (7.12×10^{-4}), and $n(CH_3)_2COO$ + HCOOH (1.27×10^{-4}) reactions by 6.22, 6.22 and 34.88 times, respectively.

A classify scheme of various organic compounds is based on their volatility, as presented by Donahue et al. (2012) The volatility of organic compounds is described by their effective saturation concentration. The saturated concentrations (c^0) of adduct products formed from the successive reactions of SCIs with HCOOH are predicted by using the SIMPOL.1 method proposed by Pankow and Asher (2008), and the results are listed in Table S10. As shown in Table S10, the c^0 of adduct products involved in the nCH_2OO + HCOOH reaction decreases with increasing the number of CH_2OO. According to the Volatility Basis Set (VBS) of organic compounds (Donahue et al.,

672   2012), these adduct products belong to VOC ($c^0 > 3 \times 10^6$ ug/m^3). Similarly, the c^0 of

673   adduct products included in the n$anti$-CH$_3$CHOO + HCOOH, nsyn-CH$_3$CHOO +

674   HCOOH, and n(CH$_3$)$_2$COO + HCOOH reactions decreases when the number of SCIs

675   increases. It deserves mentioning that the adduct products in the n$anti$-CH$_3$CHOO +

676   HCOOH and nsyn-CH$_3$CHOO + HCOOH reactions belong to intermediate volatility

677   organic compounds (IVOC, $300 < c^0 < 3 \times 10^6$ ug/m^3) when the number of SCIs is equal

678   to five. However, the adduct products in the n(CH$_3$)$_2$COO + HCOOH reaction become

679   IVOC when the number of (CH$_3$)$_2$COO is greater than or equal to two. Based on the

680   above discussions, it can be concluded that the volatility of adduct products is

681   significantly affected by the number and size of SCIs in the successive reaction of SCIs

682   with HCOOH.

4. Conclusions

684   The oligomerization reaction mechanism and kinetics of Criegee intermediates

685   reactions with their respective hydroperoxide esters as well as HPMF are investigated

686   using quantum chemical calculations and kinetics modeling methods. The main

687   conclusion is summarized as follows.

688   (a) For the initiation reactions of distinct SCIs with HCOOH, the barrierless 1,4

689   O-H insertion reaction leading to the formation of hydroperoxide esters is the most

690   favorable pathway. The exothermicity of distinct SCIs reactions with HCOOH

691   decreases when the number of methyl groups increases, and the exothermicity of the

692    $anti$-CH$_3$CHOO + HCOOH reaction is higher than that of the syn-CH$_3$CHOO +

693   HCOOH system.

694   (b) The addition reactions of SCIs with hydroperoxide esters proceed through

695   successive insertion of SCIs into hydroperoxide ester to form oligomers that involve

696   SCIs as the repeating unit. These oligomerization reactions are strongly exthermoic and

697   spontaneous. The exothermicity of oligomerization reactions significantly decreases

698   when the number of methyl substituents increases, and the exothermicity of $anti$-methyl

699   substituted carbonyl oxides is obviously higher than that of syn-methyl substituted

700   carbonyl oxides.

(c) The –OOH insertion reaction is favored over the –CH insertion pathway in the SCIs oligomerization reactions, and the barrier heights increase with increasing the number of SCIs added to the oligomer except *syn*-CH₃CHOO. The barrier of –OOH insertion pathway shows a dramatic decrease when a methyl substituent occurs at the *anti*-position, while it reveals a significant increase when a methyl group is introduced at the *syn*-position and dimethyl substituent.

(d) Compared with the barrier of CH_2OO reaction with HPMF (8.1 kcal·mol^{-1}), the barrier decreases by 2.5 kcal·mol^{-1} when a methyl substituent occurs at the *anti*-position, while the barrier increases by about 3.0 kcal·mol^{-1} when a methyl group is introduced at the *syn*-position and dimethyl substituent. The rate coefficients increase by about one order of magnitude when a methyl substituent occurs at the *anti*-position, whereas the rate coefficients decrease by 1 to 2 orders of magnitude when a methyl group is introduced at the *syn*-position compared to the rate coefficients of the CH_2OO + HPMF reaction.

Data availability

The data are accessible by contacting the corresponding author (huangyu@ieecas.cn).

Supplement

The following information is provided in the Supplement: The electronic energy ($\Delta E^{\neq}$) and Gibbs free energy ($\Delta G^{\neq}$) barriers for the initiation reactions of distinct SCIs with HCOOH predicted at different levels; Enthalpies of formation for the various carbonyl oxides and hydroperoxide esters; Rate coefficients of initiation reactions of distinct SCIs with HCOOH; Rate coefficients of distinct SCIs reactions with HPMF; Predicted saturated vapour pressure (P^0) and saturated concentrations (c^0) for the adduct products; Relaxed scan energy profiles for varying the C-O and O-H bonds in the 1,4-insertion reactions of distinct SCIs with HCOOH; Natural bond orbital (NBO) analysis

729 of the donor-acceptor orbitals; The NPA charges of different atoms in the distinct SCIs;

730 Optimized geometries of all the stationary points;

731

Author contribution

733 LC designed the study. LC and YH wrote the paper. LC performed theoretical

734 calculation. YX, ZJ, and WW analyzed the data. All authors reviewed and commented

735 on the paper.

736

Competing interests

738 The authors declare that they have no conflict of interest.

739

Acknowledgments

741 This work was supported by the National Natural Science Foundation of China

742 (grant Nos. 42175134, 41805107, and 22002080). It was also partially supported as

743 Strategic Priority Research Program of the Chinese Academy of Sciences, China (grant

744 Nos. XDA23010300 and XDA23010000), and CAS "Light of West China" Program

745 (XAB2019B01).

746

747

References

Alecu, I. M., Zheng, J., Zhao, Y., and Truhlar, D. G.: Computational thermochemistry: scale factor databases and scale factors for vibrational frequencies obtained from electronic model chemistries, J. Chem. Theory Comput., 6, 2872-2887, https://doi.org/10.1021/ct100326h, 2010.

Anglada, J. M., and Solé, A.: Impact of the water dimer on the atmospheric reactivity of carbonyl oxides, Phys. Chem. Chem. Phys., 18, 17698-17712, https://doi.org/10.1039/C6CP02531E, 2016.

Aplincourt, P., and Ruiz-López, M. F.: Theoretical study of formic acid anhydride formation from carbonyl oxide in the atmosphere, J. Phys. Chem. A, 104, 380-388, https://doi.org/10.1021/jp9928208, 2000.

Atkinson, R., and Arey, J.: Atmospheric degradation of volatile organic compounds, Chem. Rev., 103, 4605-4638, https://doi.org/10.1021/cr0206420, 2003.

Barber, V. P., Pandit, S., Green, A. M., Trongsiriwat, N., Walsh, P. J., Klippenstein, S. J., and Lester, M. I.: Four-carbon Criegee intermediate from isoprene ozonolysis: methyl vinyl ketone oxide synthesis, infrared spectrum, and OH production, J. Am. Chem. Soc., 140, 10866-10880, https://doi.org/10.1021/jacs.8b06010, 2018.

Barley, M. H., and McFiggans, G.: The critical assessment of vapour pressure estimation methods for use in modelling the formation of atmospheric organic aerosol, Atmos. Chem. Phys., 10, 749-767, https://doi.org/10.5194/acp-10-749-2010, 2010.

Boys, S. F., and Bernardi, F.: The calculation of small molecular interactions by the differences of separate total energies. Some procedures with reduced errors, Mol. Phys., 19, 553-566, https://doi.org/10.1080/00268977000101561, 1970.

Cabezas, C., and Endo, Y.: Observation of hydroperoxyethyl formate from the reaction between the methyl Criegee intermediate and formic acid, Phys. Chem. Chem. Phys., 22, 446-454, https://doi.org/10.1039/C9CP05030B, 2020.

Cabezas, C., and Endo, Y.: The Criegee intermediate-formic acid reaction explored by rotational spectroscopy, Phys. Chem. Chem. Phys., 21, 18059-18064, https://doi.org/10.1039/c9cp03001h, 2019.

Cabezas, C., and Endo, Y.: The reactivity of the Criegee intermediate CH_3CHOO with water probed by FTMW spectroscopy, J. Chem. Phys., 148, 014308-014315, https://doi.org/10.1063/1.5009033, 2018.

Canneaux, S., Bohr, F., and Henon, E.: KiSThelP: a program to predict thermodynamic properties and rate constants from quantum chemistry results, J. Comput. Chem., 35, 82-93, https://doi.org/10.1002/jcc.23470, 2013.

Caravan, R. L., Vansco, M. F., Au, K., Khan, M. A. H., Li, Y. L., Winiberg, F. A. F., Zuraski, K., Lin, Y. H., Chao, W., Trongsiriwat, N., Walsh, P. J., Osborn, D. L., Percival, C. J., Lin, J. J. M., Shallcross, D. E., Sheps, L., Klippenstein, S. J., Taatjes, C. A., and Lester, M. I.: Direct kinetic measurements and theoretical predictions of an isoprene-derived Criegee intermediate, Proc. Natl. Acad. Sci. U.S.A., 117, 9733-9740, https://doi.org/10.1073/pnas.1916711117, 2020.

Chaliyakunnel, S., Millet, D. B., Wells, K. C., Cady-Pereira, K. E., and Shephard, M. W.: A large underestimate of formic acid from tropical fires: constraints from space-borne measurements, Environ. Sci. Technol., 50, 5631-5640, https://doi.org/10.1021/acs.est.5b06385, 2016.

Chao, W., Hsieh, J. T., Chang, C. H., and Lin, J. J. M.: Direct kinetic measurement of the reaction of the simplest Criegee intermediate with water vapor, Science, 347, 751-754, https://doi.org/10.1126/science.1261549, 2015.

Chen, L., Huang, Y., Xue, Y., Cao J., and Wang, W.: Effect of oligomerization reactions of Criegee intermediate with organic acid/peroxy radical on secondary organic aerosol formation from isoprene ozonolysis, Atmos. Environ., 187, 218-229, https://doi.org/10.1016/j.atmosenv.2018.06.001, 2018.

Chen, L., Huang, Y., Xue, Y., Cao, J., and Wang, W.: Competition between HO_2 and H_2O_2 reactions with CH_2OO/*anti*-CH_3CHOO in the oligomer formation: a theoretical perspective, J. Phys. Chem. A, 121, 6981-6991, https://doi.org/10.1021/acs.jpca.7b05951, 2017.

Chen, L., Huang, Y., Xue, Y., Shen, Z., Cao, J., and Wang, W.: Mechanistic and kinetics investigations of oligomer formation from Criegee intermediate reactions with hydroxyalkyl hydroperoxides, Atmos. Chem. Phys., 19, 4075-4091, https://doi.org/10.5194/acp-19-4075-2019, 2019.

Chen, L., Wang, W., Wang, W., Liu, Y., Liu, F., Liu, N., and Wang, B: Water-catalyzed decomposition of the simplest Criegee intermediate CH_2OO, Theor. Chem. Acc., 135, 131-143, https://doi.org/10.1007/s00214-016-1894-9, 2016.

Chhantyal-Pun, R., McGillen, M. R., Beames, J. M., Khan, M. A. H., Percival, C. J., Shallcross, D. E., and Orr-Ewing, A. J.: Temperature Dependence of the Rates of Reaction of Trifluoracetic Acid with Criegee Intermediates, Angew. Chem. Int. Ed., 129, 9172-9175, https://doi.org/10.1002/anie.201703700, 2017.

Chhantyal-Pun, R., Rotavera, B., Mcgillen, M. R., Khan, M. A. H., Eskola, A. J., Caravan, R. L., Blacker, L., Tew, D. P., Osborn, D. L., Percival, C. J., Taatjes, C. A., Shallcross D. E., and Orr-Ewing, A. J.: Criegee intermediate reactions with carboxylic acids: a potential source of secondary organic aerosol in the atmosphere, ACS Earth Space Chem., 2, 833-842, https://doi.org/10.1021/acsearthspacechem.8b00069, 2018.

Chung, C. A., Su, J. W., and Lee, Y. P.: Detailed mechanism and kinetics of the reaction of Criegee intermediate CH_2OO with HCOOH investigated via infrared identification of conformers of hydroperoxymethyl formate and formic acid anhydride, Phys. Chem. Chem. Phys., 21, 21445-21455, https://doi.org/10.1039/c9cp04168k, 2019.

Criegee, R.: Mechanism of ozonolysis, Angew. Chem. Int. Ed. Engl., 14, 745-752, https://doi.org/10.1002/anie.197507451, 1975.

Donahue, N. M., Kroll, J. H., Pandis, S. N., and Robinson, A. L.: A two-dimensional volatility basis set – Part 2: Diagnostics of organic-aerosol evolution, Atmos. Chem. Phys., 12, 615-634, https://doi.org/10.5194/acp-12-615-2012, 2012.

Drozd, G. T., Kurtén, T., Donahue, N. M., and Lester, M. I.: Unimolecular decay of the dimethyl-substituted Criegee intermediate in alkene ozonolysis: decay time scales and the importance of tunneling, J. Phys. Chem. A, 121, 6036-6045, https://doi.org/10.1021/acs.jpca.7b05495, 2017.

Eckart, C.: The penetration of a potential barrier by electrons, Phys. Rev., 35, 1303-1309, https://doi.org/10.1103/PhysRev.35.1303, 1930.

Frisch, M. J., Trucks, G. W., Schlegel, H. B., Scuseria, G. E., Robb, M. A., Cheeseman, J. R., Montgomery, J. A. Jr., Vreven, T., Kudin, K. N., Burant, J. C., Millam, J. M., Iyengar, S. S., Tomasi, J., Barone, V., Mennucci. B., Cossi, M., Scalmani, G., Rega, N., Petersson, G. A., Nakatsuji, H., Hada, M., Ehara, M., Toyota, K., Fukuda, R., Hasegawa, J., Ishida, M., Nakajima,

834   T., Honda, Y., Kitao, O., Nakai, H., Klene, M., Li, X., Knox, J. E., Hratchian, H. P., Cross, J.

835   B., Adamo, C., Jaramillo, J., Gomperts, R., Stratmann, R. E., Yazyev, O., Austin, A. J., Cammi,

836   R., Pomelli, C., Ochterski, J. W., Ayala, P. Y., Morokuma, K., Voth, G. A., Salvador, P.,

837   Dannenberg, J. J., Zakrzewski, V. G., Dapprich, S., Daniels, A. D., Strain, M. C., Farkas, O.,

838   Malick, D. K., Rabuck, A. D., Raghavachari, K., Foresman, J. B., Ortiz, J. V., Cui, Q., Baboul,

839   A. G., Clifford, S., Cioslowski, J., Stefanov, B. B., Liu, G., Liashenko, A., Piskorz, P.,

840   Komaromi, I., Martin, R. L., Fox, D. J., Keith, T., Al-Laham, M. A., Peng, C. Y., Nanayakkara,

841   A., Challacombe, M., Gill, P. M. W., Johnson, B., Chen, W., Wong, M. W., Gonzalez, C., and

842   Pople, J. A.: Gaussian 09, Revision D.01; Gaussian, Inc.: Wallingford, CT, 2009.

843 Fukui, K.: The path of chemical reactions - the IRC approach, Acc. Chem. Res., 14, 363-368,

844   https://doi.org/10.1021/ar00072a001, 1981.

845 Gilbert, R. G., and Smith, S. C.: Theory of unimolecular and recombination reactions; Blackwell

846   Scientific: Carlton, Australia, 1990.

847 Giorio, C., Campbell, S. J., Bruschi, M., Tampieri, F., Barbon, A., Toffoletti, A., Tapparo, A., Paijens,

848   C., Wedlake, A. J., Grice, P., Howe, D. J., and Kalbere, M.: Online quantification of Criegee

849   intermediates of α-pinene ozonolysis by stabilization with spin traps and proton-transfer

850   reaction mass spectrometry detection, J. Am. Chem. Soc., 139, 3999-4008,

851   https://doi.org/10.1021/jacs.6b10981, 2017.

852 Glowacki, D. R., Liang, C. H., Morley, C., Pilling, M. J., and Robertson, S. H.: MESMER: an open-

853   source master equation solver for multi-energy well reactions, J. Phys. Chem. A, 116, 9545-

854   9560, https://doi.org/10.1021/jp3051033, 2012.

855 Gong, Y., and Chen, Z.: Quantification of the role of stabilized Criegee intermediates in the

856   formation of aerosols in limonene ozonolysis, Atmos. Chem. Phys., 21, 813-829,

857   https://doi.org/10.5194/acp-21-813-2021, 2021.

858 Hammond, G. S.: A correlation of reaction rates, J. Am. Chem. Soc., 77, 334-338,

859   https://doi.org/10.1021/ja01607a027, 1955.

860 Huang, H. L., Chao, W., and Lin, J. J. M.: Kinetics of a Criegee intermediate that would survive

861   high humidity and may oxidize atmospheric SO_2, Proc. Natl. Acad. Sci. U.S.A., 112, 10857-

862   10862, https://doi.org/ 10.1073/pnas.1513149112, 2015.

863 Johnson, D., and Marston, G.: The gas-phase ozonolysis of unsaturated volatile organic compounds

864   in the troposphere, Chem. Soc. Rev., 37, 699-716, https://doi.org/10.1039/B704260B, 2008.

865 Johnson, D., Lewin, A. G., and Marston, G.: The effect of Criegee-intermediate scavengers on the

866   OH yield from the reaction of ozone with 2-methylbut-2-ene, J. Phys. Chem. A, 105, 2933-

867   2935, https://doi.org/10.1021/jp003975e, 2001.

868 Karton, A., Kettner, M., and Wild, D. A.: Sneaking up on the Criegee intermediate from below:

869   Predicted photoelectron spectrum of the CH_2OO^- anion and W3-F12 electron affinity of

870   CH_2OO, Chem. Phys. Lett., 585, 15-20, http://doi.org/10.1016/j.cplett.2013.08.075, 2013.

871 Khan, M. A. H., Percival, C. J., Caravan, R. L., Taatjes, C. A., and Shallcross, D. E.: Criegee

872   intermediates and their impacts on the troposphere, Environ. Sci.: Processes Impacts, 20, 437-

873   453, https://doi.org/10.1039/C7EM00585G, 2018.

874 Lester, M. I., and Klippenstein, S. J.: Unimolecular decay of Criegee intermediates to OH radical

875   products: prompt and thermal decay processes, Acc. Chem. Res., 51, 978-985,

876   https://doi.org/10.1021/acs.accounts.8b00077, 2018.

877 Lin, J. J. M., and Chao, W.: Structure-dependent reactivity of Criegee intermediates studied with

spectroscopic methods, Chem. Soc. Rev., 46, 7483-7497, https://doi.org/10.1039/c7cs00336f, 2017.

Lin, X., Meng, Q., Feng, B., Zhai, Y., Li, Y., Yu, Y., Li, Z., Shan, X., Liu, F., Zhang, L., and Sheng, L.: Theoretical study on Criegee intermediate's role in ozonolysis of acrylic acid, J. Phys. Chem. A, 123, 1929-1936, https://doi.org/10.1021/acs.jpca.8b11671, 2019.

Liu, F., Beames, J. M., Petit, A. S., McCoy, A. B., and Lester, M. I.: Infrared-driven unimolecular reaction of CH_3CHOO Criegee intermediates to OH radical products, Science, 345, 1596-1598, https://doi.org/10.1126/science.1257158, 2014.

Liu, L., Bei, N., Wu, J., Liu, S., Zhou, J., Li, X., Yang, Q., Feng, T., Cao, J., Tie, X., and Li, G.: Effects of stabilized Criegee intermediates (sCIs) on sulfate formation: a sensitivity analysis during summertime in Beijing-Tianjin-Hebei (BTH), China, Atmos. Chem. Phys., 19, 13341-13354, https://doi.org/10.5194/acp-19-13341-2019, 2019.

Long, B., Bao, J. L., and Truhlar, D. G.: Atmospheric chemistry of Criegee intermediates: unimolecular reactions and reactions with water, J. Am. Chem. Soc., 138, 14409-14422, https://doi.org/10.1021/jacs.6b08655, 2016.

Long, B., Bao, J. L., and Truhlar, D. G.: Unimolecular reaction of acetone oxide and its reaction with water in the atmosphere, Proc. Natl. Acad. Sci. U.S.A., 115, 6135-6140, https://doi.org/10.1073/pnas.1804453115, 2018.

Long, B., Cheng, J. R., Tan, X. F., and Zhang, W. J.: Theoretical study on the detailed reaction mechanisms of carbonyl oxide with formic acid, J. Mol. Struc.: Theochem, 916, 159-167, https://doi.org/10.1016/j.theochem.2009.09.028, 2009.

Lu, T., and Chen, F.: Multiwfn: A multifunctional wavefunction analyzer, J. Comput. Chem., 33, 580-592, https://doi.org/10.1002/jcc.22885, 2012.

Mendes, J., Zhou, C. W., and Curran, H. J.: Theoretical chemical kinetic study of the H-atom abstraction reactions from aldehydes and acids by H atoms and OH, HO_2, and CH_3 radicals, J. Phys. Chem. A, 118, 12089-12104, https://doi.org/10.1021/jp5072814, 2014.

Nannoolal, Y., Rarey, J., and Ramjugernatha, D.: Estimation of pure component properties Part 3. Estimation of the vapor pressure of non-electrolyte organic compounds via group contributions and group interactions, Fluid Phase Equilibria, 269, 117-133, https://doi.org/10.1016/j.fluid.2008.04.020, 2008.

Nannoolal, Y., Rarey, J., Ramjugernatha, D., and Cordesb, W.: Estimation of pure component properties Part 1. Estimation of the normal boiling point of non-electrolyte organic compounds via group contributions and group interactions, Fluid Phase Equilibria, 226, 45-63, https://doi.org/10.1016/j.fluid.2004.09.001, 2004.

Neeb, P., Horie, O., and Moortgat, G. K.: The ethene−ozone reaction in the gas phase, J. Phys. Chem. A, 102, 6778-6785, https://doi.org/10.1021/jp981264z, 1998.

Novelli, A., Hens, K., Ernest, C. T., Martinez, M., Nölscher, A. C., Sinha, V., Paasonen, P., Petäjä, T., Sipilä, M., Elste, T., Plass-Dülmer, C., Phillips, G. J., Kubistin, D., Williams, J., Vereecken, L., Lelieveld, J., and Harder, H.: Estimating the atmospheric concentration of Criegee intermediates and their possible interference in a FAGE-LIF instrument, Atmos. Chem. Phys., 17, 7807-7826, https://doi.org/10.5194/acp-17-7807-2017, 2017.

Novelli, A., Vereecken, L., Lelieveld, J., and Harder, H.: Direct observation of OH formation from stabilised Criegee intermediates, Phys. Chem. Chem. Phys., 16, 19941-19951, https://doi.org/10.1039/c4cp02719a, 2014.

O'Meara, S., Booth, A. M., Barley, M. H., Topping, D., and McFiggans, G.: An assessment of vapour pressure estimation methods, Phys. Chem. Chem. Phys., 16, 19453-19469, https://doi.org/10.1039/C4CP00857J, 2014.

Osborn, D. L., and Taatjes, C. A.: The physical chemistry of Criegee intermediates in the gas phase, Int. Rev. Phys. Chem., 34, 309-360, https://doi.org/10.1080/0144235X.2015.1055676, 2015.

Pankow, J. F., and Asher, W. E.: SIMPOL.1: a simple group contribution method for predicting vapor pressures and enthalpies of vaporization of multifunctional organic compounds, Atmos. Chem. Phys., 8, 2773-2796, https://doi.org/10.5194/acp-8-2773-2008, 2008.

Paulot, F., Wunch, D., Crounse, J. D., Toon, G. C., Millet, D. B., DeCarlo, P. F., Vigouroux, C., Deutscher, N. M., Abad, G. G., Notholt, J., Warneke, T., Hannigan, J. W., Warneke, C., de Gouw, J. A., Dunlea, E. J., Mazière, M. D., Griffith, D. W. T., Bernath, P., Jimenez, J. L., and Wennberg, P. O.: Importance of secondary sources in the atmospheric budgets of formic and acetic acids, Atmos. Chem. Phys., 11, 1989-2013, https://doi.org/10.5194/acp-11-1989-2011, 2011.

Peltola, J., Seal, P., Inkilä, A., and Eskola, A.: Time-resolved, broadband UV-absorption spectrometry measurements of Criegee intermediate kinetics using a new photolytic precursor: unimolecular decomposition of CH_2OO and its reaction with formic acid, Phys. Chem. Chem. Phys., 22, 11797-11808, https://doi.org/10.1039/d0cp00302f, 2020.

Porterfield, J. P., Lee, K. L. K., Dell'Isola, V., Carroll, P. B., and McCarthy, M. C.: Characterization of the simplest hydroperoxide ester, hydroperoxymethyl formate, a precursor of atmospheric aerosols, Phys. Chem. Chem. Phys., 21, 18065-18070, https://doi.org/10.1039/c9cp03466h, 2019.

Riva, M., Budisulistiorini, S. H., Zhang, Z., Gold, A., Thornton, J. A., Turpin, B. J., and Surratt, J. D.: Multiphase reactivity of gaseous hydroperoxide oligomers produced from isoprene ozonolysis in the presence of acidified aerosols, Atmos. Environ., 152, 314-322, https://doi.org/10.1016/j.atmosenv.2016.12.040, 2017.

Sadezky, A., Winterhalter, R., Kanawati, B., Rompp, A., Spengler, B., Mellouki, A., Bras, G. L., Chaimbault, P., and Moortgat, G. K.: Oligomer formation during gas-phase ozonolysis of small alkenes and enol ethers: new evidence for the central role of the Criegee Intermediate as oligomer chain unit, Atmos. Chem. Phys., 8, 2667-2699, https://doi.org/10.5194/acp-8-2667-2008, 2008.

Sakamoto, Y., Inomata, S., and Hirokawa, J.: Oligomerization reaction of the Criegee intermediate leads to secondary organic aerosol formation in ethylene ozonolysis, J. Phys. Chem. A, 117, 12912-12921, https://doi.org/10.1021/jp408672m, 2013.

Sakamoto, Y., Yajima, R., Inomatad, S., and Hirokawa, J.: Water vapour effects on secondary organic aerosol formation in isoprene ozonolysis, Phys. Chem. Chem. Phys., 19, 3165-3175, https://doi.org/10.1039/c6cp04521a, 2017.

Sipilä, M., Jokinen, T., Berndt, T., Richters, S., Makkonen, R., Donahue, N. M., Mauldin Iii, R. L., Kurtén, T., Paasonen, P., Sarnela, N., Ehn, M., Junninen, H., Rissanen, M. P., Thornton, J., Stratmann, F., Herrmann, H., Worsnop, D. R., Kulmala, M., Kerminen, V. M., and Petäjä, T.: Reactivity of stabilized Criegee intermediates (sCIs) from isoprene and monoterpene ozonolysis toward SO_2 and organic acids, Atmos. Chem. Phys., 14, 12143-12153, https://doi.org/10.5194/acp-14-12143-2014, 2014.

So, S., Wille, U., and Silva, G. D.: Atmospheric chemistry of enols: a theoretical study of the vinyl

alcohol + OH + O$_2$ reaction mechanism, Environ. Sci. Technol., 48, 6694-6701, https://doi.org/10.1021/es500319q, 2014.

Stavrakou, T., Müller, J. F., Peeters, J., Razavi, A., Clarisse, L., Clerbaux, C., Coheur, P. F., Hurtmans, D., Mazière, M. D., Vigouroux, C., Deutscher, N. M., Griffith, D. W. T., Jones, N., and Paton-Walsh, C.: Satellite evidence for a large source of formic acid from boreal and tropical forests, Nat. Geosci., 5, 26-30, https://doi.org/10.1038/ngeo1354, 2012.

Taatjes, C. A., Khan, M. A. H., Eskola, A. J., Percival, C. J., Osborn, D. L., Wallington, T. J., and Shallcross, D. E.: Reaction of perfluorooctanoic acid with Criegee intermediates and implications for the atmospheric fate of perfluorocarboxylic acids, Environ. Sci. Technol., 53, 1245-1251, https://doi.org/10.1021/acs.est.8b05073, 2019.

Taatjes, C. A., Welz, O., Eskola, A. J., Savee, J. D., Scheer, A. M., Shallcross, D. E., Rotavera, B., Lee, E. P. F., Dyke, J. M., Mok, D. K. W., Osborn, D. L., and Percival, C. J.: Direct measurements of conformer-dependent reactivity of the Criegee intermediate CH$_3$CHOO, Science, 340, 177-180, https://doi.org/10.1126/science.1234689, 2013.

Taatjes, C. A.: Criegee intermediates: what direct production and detection can teach us about reactions of carbonyl oxides, Annu. Rev. Phys. Chem., 68, 183-207, https://doi.org/10.1146/annurev-physchem-052516-050739, 2017.

Tobias, H. J., and Ziemann, P. J.: Kinetics of the gas-phase reactions of alcohols, aldehydes, carboxylic acids, and water with the C13 stabilized Criegee intermediate formed from ozonolysis of 1-tetradecene, J. Phys. Chem. A, 105, 6129-6135, https://doi.org/10.1021/jp004631r, 2001.

Truhlar, D. G., Hase, W. L., and Hynes, J. T.: Current status of transition-state theory, J. Phys. Chem., 87, 2664-2682, https://doi.org/10.1021/jp953748q, 1996.

Vansco, M. F., Zuraski, K., Winiberg, F. A. F., Au, K., Trongsiriwat, N., Walsh, P. J., Osborn, D. L., Percival, C. J., Klippenstein, S. J., Taatjes, C. A., Lester, M. I., and Caravan, R. L.: Functionalized hydroperoxide formation from the reaction of methacrolein-oxide, an isoprene-derived Criegee intermediate, with formic acid: experiment and theory, Molecules, 26, 3058-3072, https://doi.org/10.3390/molecules26103058, 2021.

Vereecken, L., Harder, H., and Novelli, A.: The reaction of Criegee intermediates with NO, RO$_2$, and SO$_2$, and their fate in the atmosphere, Phys. Chem. Chem. Phys., 14, 14682-14695, https://doi.org/10.1039/c2cp42300f, 2012.

Vereecken, L.: The reaction of Criegee intermediates with acids and enols, Phys. Chem. Chem. Phys., 19, 28630-28640, https://doi.org/10.1039/c7cp05132h, 2017.

Wang, S., Newland, M. J., Deng, W., Rickard, A. R., Hamilton, J. F., Muñoz, A., Ródenas, M., Vázquez, M. M., Wang, L., and Wang, X.: Aromatic photo-oxidation, a new source of atmospheric acidity, Environ. Sci. Technol., 54, 7798-7806, https://doi.org/10.1021/acs.est.0c00526, 2020.

Welz, O., Eskola, A. J., Sheps, L., Rotavera, B., Savee, J. D., Scheer, A. M., Osborn, D. L., Lowe, D., Booth, A. M., Xiao, P., Khan, M. A. H., Percival, C. J., Shallcross, D. E., and Taatjes, C. A.: Rate coefficients of C(1) and C(2) Criegee intermediate reactions with formic and acetic Acid near the collision limit: direct kinetics measurements and atmospheric implications, Angew. Chem. Int. Ed., 53, 4547-4550, https://doi.org/10.1002/anie.201400964, 2014.

Welz, O., Savee, J. D., Osborn, D. L., Vasu, S. S., Percival, C. J., Shallcross, D. E., and Taatjes, C. A.: Direct kinetic measurements of Criegee intermediate (CH$_2$OO) formed by reaction of CH$_2$I

1010   with O_2, Science, 335, 204-207, https://doi.org/10.1126/science.1213229, 2012.

1011   Yin, C., and Takahashi, K.: How does substitution affect the unimolecular reaction rates of Criegee
1012   intermediates?   Phys.   Chem.   Chem.   Phys.,   19,   12075-12084,
1013   https://doi.org/10.1039/c7cp01091e, 2017.

1014   Yu, S.: Role of organic acids (formic, acetic, pyruvic and oxalic) in the formation of cloud
1015   condensation   nuclei   (CCN):   a   review,   Atmos.   Res.,   53,   185-217,
1016   https://doi.org/10.1016/S0169-8095(00)00037-5, 2000.

1017   Zhang, P., Wang, W., Zhang, T., Chen, L., Du, Y., Li, C., and Lv, J.: Theoretical study on the
1018   mechanism and kinetics for the self-reaction of $C_2H_5O_2$ radicals, J. Phys. Chem. A, 116, 4610-
1019   4620, https://doi.org/10.1021/jp301308u, 2012.

1020   Zhao, R., Kenseth, C. M., Huang, Y., Dalleska, N. F., Kuang, X. M., Chen, J., Paulson, S. E., and
1021   Seinfeld, J. H.: Rapid aqueous-phase hydrolysis of ester hydroperoxides arising from Criegee
1022   intermediates   and   organic   acids,   J.   Phys.   Chem.   A,   122,   5190-5201,
1023   https://doi.org/10.1021/acs.jpca.8b02195, 2018.

1024   Zhao, Y., and Truhlar, D. G.: The M06 suite of density functionals for main group thermochemistry,
1025   thermochemical kinetics, noncovalent interactions, excited states, and transition elements: two
1026   new functionals and systematic testing of four M06-class functionals and 12 other functionals,
1027   Theor. Chem. Acc., 120, 215-241, https://doi.org/10.1007/s00214-007-0310-x, 2008.

1028   Zhao, Y., Wingen, L. M., Perraud, V., Greaves, J., and Finlayson-Pitts, B. J.: Role of the reaction of
1029   stabilized Criegee intermediates with peroxy radicals in particle formation and growth in air,
1030   Phys. Chem. Chem. Phys., 17, 12500-12514, https://doi.org/10.1039/c5cp01171j, 2015.

1031   Zhou, S., Joudan, S., Forbes, M. W., Zhou, Z., and Abbatt, J. P. D.: Reaction of condensed-phase
1032   Criegee intermediates with carboxylic acids and perfluoroalkyl carboxylic acids, Environ. Sci.
1033   Technol. Lett., 6, 243-250, https://doi.org/10.1021/acs.estlett.9b00165, 2019.